2022

LOAD AND PRESSURE DISTRIBUTION AS A FUNCTION OF DYNAMIC CONTACT STRESS AT THE RAILROAD CROSSTIE-BALLAST INTERFACE

Habib Abdil Unluoglu
University of Kentucky, hun222@uky.edu
Digital Object Identifier: https://doi.org/10.13023/etd.2022.362

STUDENT AGREEMENT:

I represent that my thesis or dissertation and abstract are my original work. Proper attribution has been given to all outside sources. I understand that I am solely responsible for obtaining any needed copyright permissions. I have obtained needed written permission statement(s) from the owner(s) of each third-party copyrighted matter to be included in my work, allowing electronic distribution (if such use is not permitted by the fair use doctrine) which will be submitted to UKnowledge as Additional File.

I hereby grant to The University of Kentucky and its agents the irrevocable, non-exclusive, and royalty-free license to archive and make accessible my work in whole or in part in all forms of media, now or hereafter known. I agree that the document mentioned above may be made available immediately for worldwide access unless an embargo applies.

I retain all other ownership rights to the copyright of my work. I also retain the right to use in future works (such as articles or books) all or part of my work. I understand that I am free to register the copyright to my work.

REVIEW, APPROVAL AND ACCEPTANCE

The document mentioned above has been reviewed and accepted by the student's advisor, on behalf of the advisory committee, and by the Director of Graduate Studies (DGS), on behalf of the program; we verify that this is the final, approved version of the student's thesis including all changes required by the advisory committee. The undersigned agree to abide by the statements above.

Habib Abdil Unluoglu, Student

Dr. L. Sebastian Bryson, Major Professor

Dr. Mei Chen, Director of Graduate Studies

LOAD AND PRESSURE DISTRIBUTION AS A FUNCTION OF DYNAMIC CONTACT STRESS AT THE RAILROAD CROSSTIE-BALLAST INTERFACE

THESIS

A thesis submitted in partial fulfillment of the
requirements for the degree of Master of Science in the
College of Engineering
at the University of Kentucky

By

Habib Abdil Unluoglu

Lexington, Kentucky

Co- Directors: Dr. L. Sebastian Bryson, Professor of Civil Engineering

and Dr. Jerry G. Rose, Professor of Civil Engineering

Lexington, Kentucky

2022

[https://orcid.org/0000-0001-2345-6789]

ABSTRACT OF THESIS

LOAD AND PRESSURE DISTRIBUTION AS A FUNCTION OF DYNAMIC CONTACT STRESS AT THE RAILROAD CROSSTIE-BALLAST INTERFACE

Excessive crosstie wear and abrasion and ballast wear and fouling are two of the fundamental problems contributing to inadequate railroad track performance. This adversely affects the attainment and long-term maintenance of desired track geometric requirements. The magnitudes and distribution of the stresses at the crosstie-ballast (CT-B) interface must be known to determine the stress distribution on the ballast. However, the stresses at the top of the ballast often vary significantly. This study examines a new approach to predicting dynamic contact pressures at the interface of crosstie and ballast using the 'square wave theory.' A data set of in-track CT-B interfacial pressures, taken from a freight mainline in Mascot, TN limited to speeds up to 64 km/h, in 2018, was analyzed to develop relationships in the form of equations to predict dynamic contact pressures as a function of specific information, including train speed, weight, number of axles, and wheel spacing. Several equations were developed to predict CT-B interfacial pressures as a function of these variables. Additionally, the developed square wave theory and obtained data are analyzed and compared to traditional recommended design practices. Longitudinal stress distribution over the crossties and the stress distribution along the crossties are presented. Based on the analyzed CT-B interfacial pressures, the ballast stress distribution is discussed, and recommendations are made.

KEYWORDS: railroad, crosstie, ballast, square wave theory, stress distribution, trackbed pressures

Habib Abdil Unluoglu

(Name of Student)

08/03/2022

Date

LOAD AND PRESSURE DISTRIBUTION AS A FUNCTION OF DYNAMIC CONTACT STRESS AT THE RAILROAD CROSSTIE-BALLAST INTERFACE

By
Habib Abdil Unluoglu

Dr. L. Sebastian Bryson
Co-Director of Thesis

Dr. Jerry G. Rose
Co-Director of Thesis

Dr. Mei Chen
Director of Graduate Studies

08/03/2022
Date

ACKNOWLEDGMENTS

I wish to express my deepest appreciation to my committee chair, Professor L. Sebastian Bryson, who has the attitude and the substance of a genius: he continually and convincingly conveyed a spirit of adventure regarding research and excitement regarding teaching. Without his guidance and persistent help, this thesis would not have been possible.

I owe and respectfully offer my thanks to my co-supervisor, Professor Jerry G. Rose, who introduced me to the University of Kentucky, and whose enthusiasm for the railroad had a lasting effect. I also thank Professor Rose for permission to include his research data in my thesis. His guidance and supervision played a pivotal role in the success of my academic goals. This thesis is the result of his painstaking and generous attitude.

I would like to express my thanks to my committee member, Professor Michael Kalinski, who gave me valuable time and support in all aspects.

I am thankful to the Turkish government and the Ministry of Education for their financial support.

Last but not least, I wish to convey my thanks to Michael Edelen and Mehmet Gursu for proofreading, Huseyin Cinar for programming, and all who are concerned directly or indirectly for helping me in the successful completion of this thesis.

TABLE OF CONTENTS

LIST OF TABLES

LIST OF FIGURES

1 **INTRODUCTION**

1.1 PROBLEM STATEMENT

Railroad tracks are typically designed to be cost-effective and easily maintained. This is the practice for lines in the United States used primarily for freight trains. To optimize design practices for achieving a high-quality track, it is essential to understand the fundamental behaviors of the primary components of the railroad track.

Ballast is one of the fundamental components of the track structure and often accounts for a substantial amount of expense accumulated during routine maintenance activities and periodic renewals (Huang and Qiu 2018). The ballast gets denser, and aggregate degradation or permeant deformations occur due to the loads transferred from the wheel-rail contact surface through the rail, crosstie plate, and crosstie to the ballast. Ballast particles gradually degrade, producing fine particles known as 'fouled' ballast. As the ballast particles impinge on the crossties and against each other during cyclic loadings, degradation occurs in the weaker ballast material, fine-size dust (fouling) is produced, and the particles spread laterally underneath the crossties causing permanent deformations of the railroad track (Lobo-Guerrero and Vallejo 2006). More specifically, a better understanding of stress distribution through ballast will contribute to optimizing track design practices and track and trackbed performance. However, the stresses acting at the top of the ballast, the crosstie-ballast (CT-B) interface, must be determined to comprehend the stress distribution through the ballast and supporting layers.

Measuring the stresses on the CT-B interface is necessary for determining the distribution of the pressures throughout the ballast. The recommended practices of the American Railway Engineering and Maintenance-of-Way Association (AREMA) are

primarily based on the Talbot (1940) methodology equations. The Talbot equations were developed in the 1920s to 1940s for jointed rail trackbed and rail traffic loadings of that era. These empirical equations (Talbot 1940) were based on a variety of assumptions requiring inputs such as dynamic load factor and wheel diameter and may not be applicable for modern-day freight train operations. (Thompson et al. 2020).

For typical CT-B design practices, AREMA (2018) recommends maximum CT-B interfacial pressures of 450 kPa for wood crossties and 585 kPa for concrete crossties. This design practice assumes that the pressures are distributed over the outer two-thirds of the crosstie, and 40% of the wheel load is equally distributed by the crosstie directly under the wheel. Additionally, the data used to develop this traditional design practice (Talbot 1940) was obtained for jointed rail track. The joint in the rail contributes significant impact loading by generating dynamic wheel loadings as the rail crosses (jumps) the gap or joint where the individual rails are joined. Much of this dynamic effect is due to differential vertical rail and support conditions (Li et al. 2016). This traditional design methodology (Talbot 1940) is dated relative to determining contact pressures at the CT-B interface. The uncertainty of the stresses at the CT-B interface may be misleading for understanding abrasion and stress distribution through the ballast. Another popular method commonly used by some railroad consulting firms to determine vertical stresses in the railroad track is the Ahlf (2003) methodology. Ahlf (2003) stated that the current AREMA recommended maximum stress (170 kPa) at the bottom of the ballast is grossly in excess. Therefore, a new approach is desired to further quantify dynamic contact pressures at the CT-B interface. This thesis hypothesizes that the crosstie-ballast (CT-B) interfacial pressures due to a moving train can be described using arbitrary pulses or waves. This

research provides data, limited to 64 km/h, for the dynamic stresses at the CT-B interface. The necessary data set is obtained thanks to the Federal Railroad Administration research test trains in Mascot, TN in 2018. The dataset was collected using 230 mm diameter hydraulic pressure cells specifically designed to measure pressures in granular material like ballast (Russell et al. 2020). This collected data set is used in this thesis to develop a new approach to predicting the dynamic contact pressures at the CT-B interface.

The new approach reported herein, developed relationships in the form of equations to predict contact stresses as a function of specific information, including train speed, weight, number of axles, and wheel spacing.

Additionally, this research investigates the longitudinal pressure distribution along the track from single wheel loads and compares it with the current recommended practice. Multiple tests were conducted at various speeds and wheel loads to measure pressure magnitudes and distribution. Therefore, knowing the longitudinal stress distribution assists in developing an improved design system. Another topic investigated by this research is the relative distribution and magnitudes of pressures along the length of the crosstie. The Talbot (1940) procedure assumes that the load distribution along the crosstie is uniform, with the outer two-thirds of the crosstie equally distributing the loads (Hay 1982).

The traditional method (Talbot 1940) has limitations for determining the stresses at the CT-B interface, and stresses calculated by using this method (Talbot 1940) are significantly overestimated measured values. Therefore, the stresses at the bottom of the ballast have been overestimated as well. The pressure distribution through the ballast, based on the new method predictions at the CT-B interface, is evaluated for this research.

1.2 OBJECTIVES

This study investigates the dynamic contact pressures at the CT-B interface for consideration to be included for upgrading recommended design practices (AREMA 2018). Geokon Granular Material Pressure Cells are an advanced data acquisition technology providing a simple and reliable measurement to obtain the pressures in granular material such as ballast. The technical specifications of Geokon Granular Material Pressure Cells (GMPCs) and the calibration report are shown in Appendix A. The identified objectives of this research are:

1. To predict the dynamic pressures at the crosstie-ballast (CT-B) interface by using a new approach developed by analyzing the data of the Federal Railroad Administration (FRA) test train set.
2. To extend the knowledge of the dynamic contact pressures at the CT-B interface and to understand the stress distribution in railroad trackbeds.
3. To develop a new approach known as, the square wave methodology to predict dynamic contact stress at the CT-B interface for any given basic information consisting of speed, train car weights, number of axles, and wheel spacings for an unlimited number of trains.
4. To propose equations to predict static and crosstie and ballast interfacial dynamic contact pressures.
5. To predict the affected distances due to wheel loadings at various speeds.
6. To propose equations to determine the static and dynamic affected distances due to the wheel loadings with respect to the analyzed measured data.
7. To dispute the general assumption that the dynamic pressures increase with speed limited to 64 km/h.

8. To extend the knowledge of the pressure distribution along the crosstie.

9. To extend the knowledge of the longitudinal stress distribution over crossties.

10. To dispute the general assumption that the crosstie is analyzed as a square footing for the ballast stress distribution.

11. To compare the differences among the recommended practice methods, the square wave method, and the measured data.

12. To give recommendations based on the dissimilarities between recommended practices and obtained data set results.

13. To support the Ahlf recommendation report for the AREMA Manual.

14. To recommend that finite element models consider wheel spacing and crosstie spacing for determining vertical stresses in railroad track.

1.3 CONTENTS OF THESIS

Chapter 1: Introduction containing the problem statement and the objectives of the thesis. Note that Chapter 2 and Chapter 3 represent two technical journal papers to be submitted from this work. Consequently, Chapters 2 and 3 are the journal papers, verbatim.

Chapter 2: A new approach to predict dynamic contact pressures at the crosstie-ballast (CT-B) interface with the basic information consisting of the number of trains, speeds, train car weights, number of axles, and distances between wheels. The mentioned theory can be applied to an unlimited number of trains. This chapter also proposes equations to predict static contact pressures and predicts affected distances due to the wheel loadings. The square wave theory is used to predict the dynamic contact pressures and affected distance magnitudes. Subsequently, the predictions are plotted to project them in square

wave shapes. Lastly, the plots are compared to the actual in-track measured data in order to confirm the adequacy of the program.

Chapter 3: A successful method for measuring dynamic contact pressure magnitudes at the CT-B interface is presented. Additionally, Chapter 3 compares the recommended practices using the Talbot (1940) method, the Ahlf (2003) method, and the square wave theory pressures to the real-time measured data obtained from FRA test trains in Mascot, TN in 2018. The longitudinal pressure distribution over the crossties and the load/pressure distribution of the single wheel load along the crosstie positioned on an all-granular trackbed are also discussed in this chapter. The traditional Talbot (1919) stress distribution method is compared to the real-time measured data set, and the dissimilarities between them are discussed. Additionally, the stress distribution on ballast and common design assumptions are discussed, and recommendations are made based on the findings and the conclusions of the study.

Chapter 4: The concluding chapter summarizes the combined findings and conclusions emanating from the research.

PREDICTING DYNAMIC CONTACT STRESSES AT CROSSTIE-BALLAST INTERFACE BASED ON BASIC INFORMATION OF TRAINS

ABSTRACT

Railroad track is designed to be cost-effective and easily maintained. Understanding fundamental track behaviors under dynamic load conditions is important to optimize design practices and achieve high-quality track performance. The recommended practices of the American Railway Engineering and Maintenance-of-Way Association (AREMA) to analyze track stresses are primarily based on Talbot Methodology equations. The unreliability of the pressure capsules used during the testing procedure, inconsistent supporting conditions, the use of jointed rails, the sensitivity of monitoring wheel and rail irregularities, improved track designs (asphalt layer), increased traffic demand, and wheel loads may be shown as primary reasons that the Talbot Methodology may not be valid for the current railroads in the U.S. Therefore, measuring the pressures at the crosstie-ballast (CT-B) interface is necessary for determining the distribution of the stresses throughout the ballast. A dataset of in-track CT-B interfacial pressures, limited to 64 km/h, taken from a freight mainline in Mascot, TN in 2018, was analyzed to develop relationships in the form of equations to predict contact stresses as a function of specific information, including train speed, train weights, number of axles, wheel spacing. Several equations were developed to predict CT-B interfacial contact pressures as a function of these variables.

KEYWORDS: Railroad, Trackbed Pressure, Dynamic Contact Stresses, Square Wave Theory, Crosstie, Ballast.

2 PREDICTING DYNAMIC CONTACT STRESSES AT CROSSTIE-BALLAST INTERFACE BASED ON BASIC INFORMATION OF TRAINS

2.1 INTRODUCTION

Loads are transferred from wheel-rail contact through the crosstie and ballast with descending values of stress magnitude. It is important to know how much loss occurred during the load transfer from the rail-wheel interface to the CT-B interface. However, the amount of loss is uncertain. The uncertainty of determining the dynamic pressures at the crosstie-ballast (CT-B) interface and the stress distribution through the ballast have been issues of concern for the railroad industry. Since the ballast is one of the fundamental components of the railroad track, a significant amount of the track maintenance expenses relates to maintaining an adequate layer of ballast. Chrismer and Davis (2000) estimated approximately $500 million annually is expended for 150,000 km of Class I track [roughly $3800/(km·year)].

The Talbot (1940) method, developed during the early 1900s, was the pioneering method used to analyze railroad track pressures. Although this method (Talbot 1940) is still the recommended design practice in the United States (AREMA 2018), the Talbot (1940) methodology is outdated for the current railroad industry. Watts and Rose (2018) state the instrumentation and measurement methodologies utilized to develop the Talbot (1940) method are out-of-date compared to current track advancements and the availability, and current hydraulic pressure sensors. On the other hand, Van Dyk et al. (2014) notes that the design guidelines in North America may not be valid for current traffic conditions, axle loads, or other conditions. These researchers state that further research on track components performed over the last several decades raises the question that the recommended design guidelines (AREMA 2018) might be questionable. The unreliability

of the pressure capsules used during the Talbot (1940) testing procedure, inconsistent supporting conditions, the use of jointed rails, the sensitivity of monitoring wheel and rail irregularities, improved track designs (asphalt layer), increased traffic volumes, higher wheel loads, and other reasons represent additional primary reasons.

A new approach is desirable to measure more reliable pressure magnitudes. The pressures should be measured with a suitable and advanced device to develop this new approach. Russell et al. (2020) conducted comprehensive field measurements at various wheel loadings and train speeds to investigate the dynamic contact stresses at the crosstie-ballast (CT-B) interface in Mascot, TN. The summarized percentage of pressure distribution of a single wheel load on an all-granular trackbed is shown in Figure 2.1 based on in-track pressure measurements.

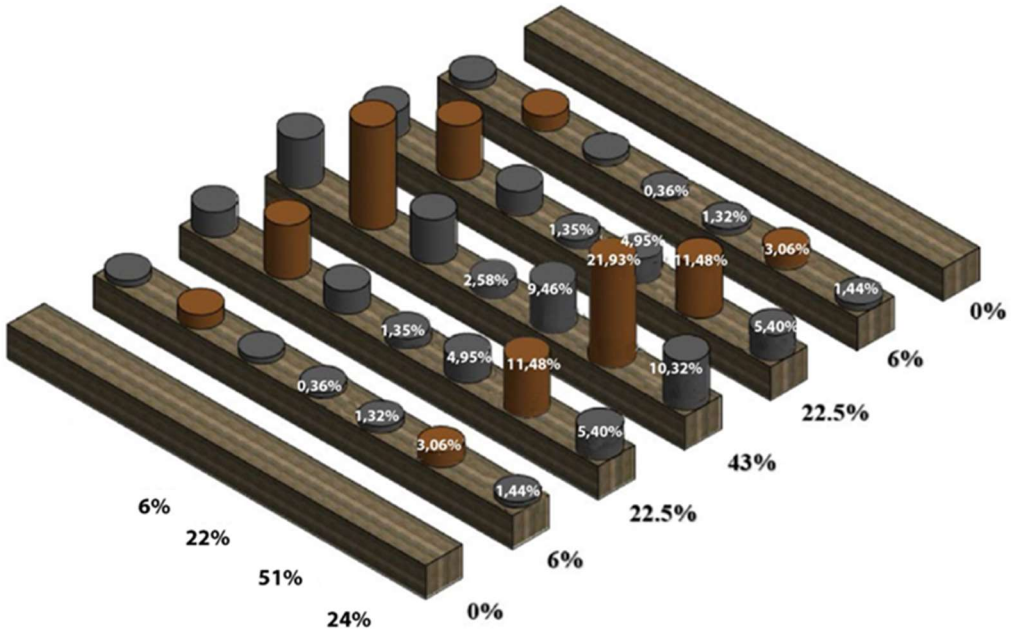

Figure 2.1 Percentage of pressure distribution of a single wheel load on an all-granular trackbed (after Russell et al. 2020).

Pressure at the crosstie-ballast (CT-B) interface due to a moving train can be approximated using square wave theory. Each wheel transfers loads to the supporting layers of a railroad by passing through the rail, crosstie pad, crosstie, and ballast. Since trucks (bogies) are located under the ends of a railway vehicle with four or six wheels, square waves may be used to the pressures due to trucks.

This paper uses the data set obtained from the Russell et al. (2020) research. However, it is important to note that the pressures were measured at various speeds limited to 64 km/h. This paper analyzes the aforementioned data to predict CT-B interfacial dynamic contact pressures and proposes equations for static and dynamic pressures. A square wave theory is used to predict dynamic pressures at the CT-B interface. A methodology review follows in order to further describe the concept.

2.2 THE SQUARE WAVE THEORY

The pressures on the components of the railroad infrastructure are functions of several variables, such as the static loadings, train speed, and the distribution of the static loads. The general assumption in the railroad industry is that the distributions of the loads on wheels are equal magnitudes. However, it is more likely to rely on the location of the centroid. For instance, if the engine of the locomotive is not located directly in the center of the locomotive, the load distributions on each wheel will be different. Unfortunately, little information in the literature is available about determining the wheel load distributions for railroad vehicles. In light of this deficit, the assumption that wheel loads are equally distributed is assumed valid in this paper.

An ideal pulse can be described with three elements, which are “rising edge”, “amplitude”, and “falling edge”. An impulse is any signal that is completely zero except

for a short signal of arbitrary shape (Smith 2013). The distance between the rising edge and the falling edge is expressed as “pulse width”. A square function, which can be called a pulse wave as well, is a periodic waveform that is a form of rapid transition between two points. Therefore, a square wave can be envisioned as a long impulse. Figure 2.2 illustrates the elements of an ideal pulse.

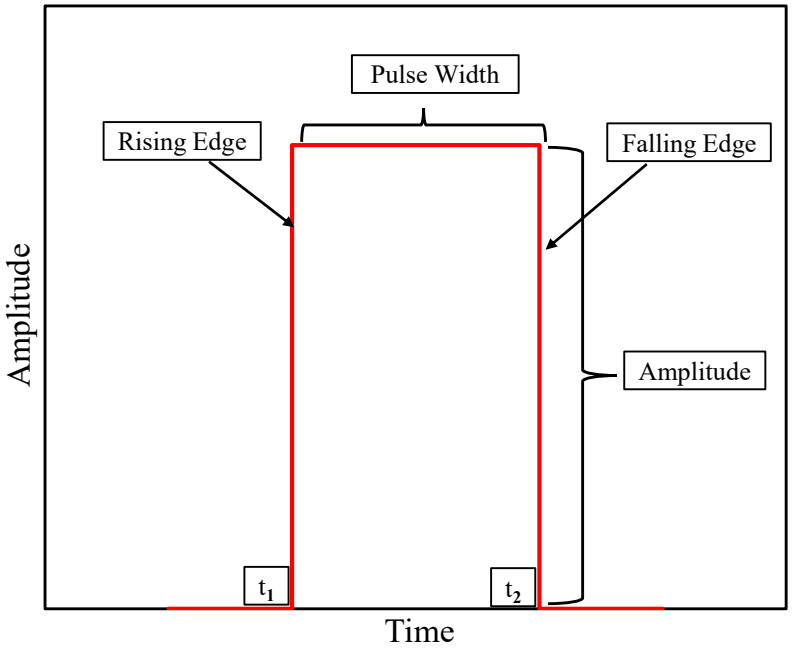

Figure 2.2 The elements of an ideal pulse.

The amplitude is described as the distance displaced from its equilibrium position. The terms t_1 and t_2 represent the rising and falling times, respectively.

In this paper, the square wave theory is used to predict the dynamic contact pressures at the CT-B interface. Specifically, the amplitude represents the average dynamic pressure due to the wheel loadings of each bogie. The assumption is that the loads are uniformly distributed through the wheels. Subsequently, the predicted amplitudes will illustrate the dynamic pressures produced by each truck. The width of the square waves

can be depicted by the wheel spacings. Specifically, the pulse width represents the length of the trucks.

2.3 THE ANALYSIS OF THE DATASET

Analyzing the root causes of the irregularities on the track is momentous since any design problem will require maintenance. Maintenance is not always a successful solution if the maintenance does not solve the root problems (Li et al. 2016). The root problems result from the pressures acting on the railroad track. These problems tend to cause track geometry deteriorations and ballast fouling (Indraratna et al. 2011). Therefore, understanding the stresses acting on the track is essential to reduce the amount of maintenance, and the stresses through the ballast should be examined. However, the stresses at the top of the ballast, which is the CT-B interface, should be determined as well in order to improve the knowledge of the stress distribution through the ballast.

Russell et al. (2020) noticed this issue and conducted tests to measure the real-time dynamic pressures at the CT-B interface. The tests were conducted at various speeds such as 3 km/h, 16 km/h, 32 km/h, 48 km/h and 64 km/h to determine the effect of speed on the CT-B interfacial dynamic contact pressures. Federal Railroad Administration (FRA) Comprehensive Inspection and Test Trains shown in Figure 2.3 were used through the testing process. FRA test trains consisted of a 6-axle NS SD60E Diesel-Electric Locomotive, DOTX 218 test car used mainly to measure vertical track stiffness and gage restraint, and DOTX 220 inspection car used primarily to measure ride quality and track geometry. The NS SD60E Diesel-Electric Locomotive had a wheel load of 147 kN, the DOTX 220 inspection car had nominal wheel loads of 118 kN, and the DOTX 218 test car had various wheel loads depending on the magnitude of the deployable axle load. The

deployable axle produced a wheel load of 98 kN, while the remaining axles of the DOTX 218 test car had wheel loads of 77 kN for the run-through tests. Earth pressure cells were placed at the CT-B interface on an active track in Mascot, TN. The study used a procedure to limit changes in the existing ballast conditions during placement of the earth pressure cells. A double tamping procedure was performed to ensure the contact surfaces were uniform. High-grade railroad rail type 136 RE continuous welded rail was secured with cut spike fasteners to timber crossties. The crosstie spacing from center to center was 508 mm. Each crosstie was box anchored. The ballast was clean, and no indications of mud or fouling had been reported. The wheels of the train were smooth enough to minimize any undesired impact loadings (Russell et al. 2020).

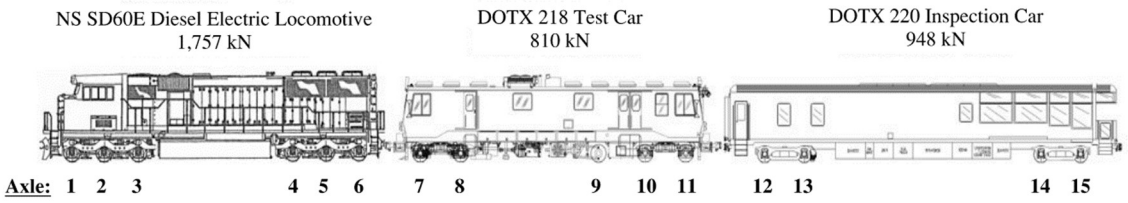

Figure 2.3 Drawing of FRA test trains, diesel-electric locomotive, test car and inspection car, respectively (after Russell et al. 2020).

However, this research can be extended, and the data collected can be used to determine dynamic contact stresses at the CT-B interface at any given speed, at any wheel loading, and for any number of trains. The steps to analyze the data obtained from the FRA test trains are represented in this paper.

2.3.1 Predicting the Static Contact Pressures

The static wheel loads should be known to predict static contact pressures since the stress is the force acting on per unit area. Static loading consists of two components. The first component is the live load, which is the weight of the train, and the second one is the

dead load, which is the weight of the subgrade and track (Li et al. 2016). Since the live load is the most dominant component, it will be the focus of this paper.

The stress distribution produced by the weight of the train is different with depth, unlike the stress distribution produced by the weight of the track and subgrade. The Boussinesq (Das et al. 2019) solution for a vertical point load applied to the surface is often used to determine the stresses at any point inside. The Boussinesq (Das et al. 2019) solution assumes a homogeneous, elastic, and isotropic material. The vertical stress at the CT-B interface is determined using the Boussinesq Point Load Equation. However, the Boussinesq Point Load Equation is not valid for railroad. The main reason why this equation is not valid is that the Boussinesq (Das et al. 2019) method assumes homogenous material.

There are significant losses during the transfer of pressures from wheel to rail, rail to rail seat, rail seat to crosstie, and crosstie to ballast. Therefore, computer models such as GEOTRACK (Transportation Technology Center INC) and KENTRACK (Liu and Rose 2013) were developed to determine the vertical pressures. These models are three-dimensional, multi-layer models for determining the responses of the track and subgrade as a function of the axle loads, rail and crosstie properties, crosstie spacing, and so on. Both models are finite element models based on the multiple degree-of-freedom spring systems. The American railroad industry recommends the Talbot (1940) methodology to determine railroad track pressures. Additionally, Ahlf (2003) wrote a report including comments on the AREMA Manual about the analysis of vertical stresses in the railroad track. The Ahlf (2003) methodology is one of the methods commonly used by some railroad consultant firms to determine the vertical pressures in a railroad track. Ahlf (2003) stated that the

current AREMA recommended maximum stress (170 kPa) at the bottom of the ballast is grossly in excess of the measured stresses. The results of this paper concur the finding of the Ahlf (2003) study. More specifically, the current research shows the pressures at the CT-B interface are overestimated by the Talbot (1940) method.

The Ahlf (2003) method considers the rail an elastic beam like many other approaches (e.g., Talbot 1918; Timoshenko 1927; and Raymond 1985). Hence, the modulus of elasticity of rail support is important. The modulus of elasticity of rail support can be described as the pressure per unit of each rail required to depress the track one unit (Powrie and Le Pen 2016). It quantifies the crosstie, ballast, and subgrade stiffness as a system. There are other indexes of combinations such as crosstie spacing and dimensions, ballast quality and so on (Ahlf 2011). Table 2.1 presents the presumptive track modulus values for different track types:

Table 2.1 Track Modulus values for different track types (Ahlf, 2011).

Track Type	Track Modulus (MPa)
Very Poor Track	3.45
Poor Track	6.89
Averaged Wood-Tie Track	13.79
Good Wood-Tie Track	20.68
Very Stiff Wood-Tie Track	34.47
Concrete-Tie Track	48.26 – 55.16

The average of Good Wood-Tie Track and Very Stiff Wood-Tie Track, 27.6 MPa, has been used as a track modulus to calculate static vertical pressures at the CT-B interface. The pressure that crosstie exerts on the ballast can be found:

$$P_a = \frac{TP_V S}{LB} \cdot \left(\frac{U}{4EI} \right)^{1/4} \quad (1)$$

where P_a is the pressure at the CT-B interface; T is the relative value multiplier; P_V is the dynamic load per wheel; S is center-to-center spacing; L and B are the length and width of the crosstie, respectively; U is track modulus; E and I stand for the elastic modulus of rail and moment of inertia of the rail, respectively (Ahlf 2011).

The CT-B interfacial static pressures were calculated for each wheel load. The assumptions, input parameters, and the steps of the calculations are shown in Appendix B. The calculations were made by using the software called Mathcad 7.0 Prime (PTC 2021). However, it is possible to develop a more straightforward equation to estimate those pressures based on the measured data. The CT-B interfacial pressures were measured to extend the knowledge of the stress distribution in the railroad track, and Table 2.2 shows the data measured at various train speeds and wheel loads. It is noted that the maximum train speed was 64 km/h for the obtained data.

Table 2.2 Measured dynamic contact pressures at different speeds and wheel loads.

Wheel Loads (kN)	Pressures (kPa) at different speeds				
	3.2 km/h	16.1 km/h	32.2 km/h	48.3 km/h	64.4 km/h
76.7	51.7	51.0	47.6	48.9	39.3
97.9	62.1	60.7	62.7	58.6	54.5
118.4	126.2	124.8	126.2	122.7	111.7
146.8	188.9	184.1	178.6	174.4	162.7

Pressure magnitudes corresponding to the real-time measured data from Table 2.2 are significantly less than AREMA (2018) trackbed design recommendation magnitudes.

The significant differences may be relevant to multiple assumptions made in the traditional method (Talbot 1940). For instance, the Talbot method (1940) states that the dynamic contact pressure increases once the speed increases. However, it is shown in Table 2.2 that the dynamic pressure decreases slightly at the interface of crosstie and ballast by speeding up to 64 km/h. The reliability of measurement devices, inconsistent supporting conditions, track/wheel irregularities, and other subjects may also explain the significant difference. Therefore, a new approach is desirable to estimate the contact stresses at the CT-B interface. This section analyzes the measured pressures to develop simple equations to predict dynamic contact stresses at the CT-B interface.

As the trends of the dynamic pressures are found subject to wheel loadings, the intercepts of the trendlines will be the static pressures. Specifically, the pressures at 0 km/h can be determined by projecting the trend of the measured data at each speed and wheel load. Figure 2.4 illustrates the trend of the pressures at different wheel loads at different speeds. The linear regression of the data is in the form of:

$$y = mx + b \tag{2}$$

where y is the pressure in kPa; x is the speed in km/h; m is the slope of the line; b is the intercept.

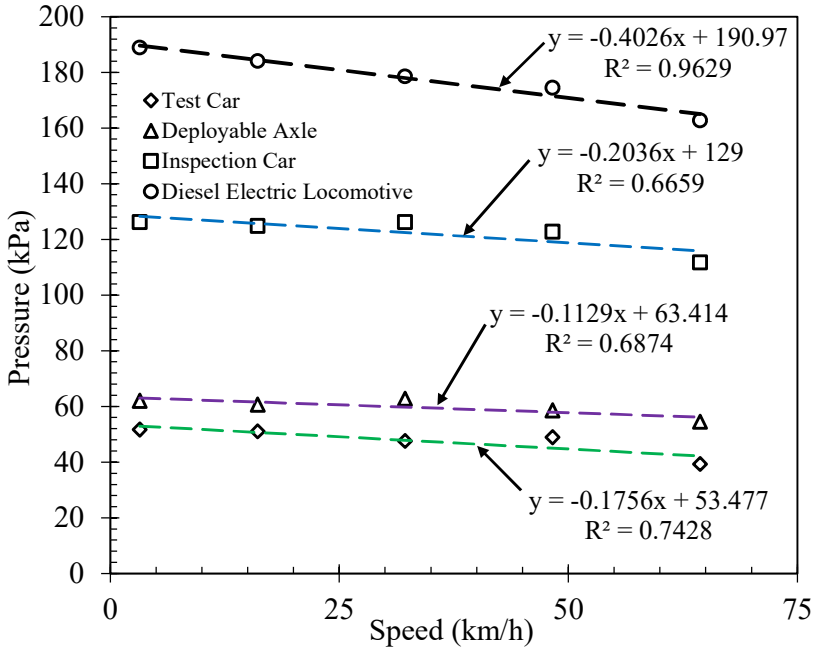

Figure 2.4 The trends for different wheel loads at different speeds.

The intercepts of trendlines illustrate the static pressures at the CT-B interface. The corresponding static pressures to wheel loads are shown in Table 2.3.

Table 2.3 Corresponding static pressures at different wheel loads.

Wheel Loads (kN)	Pressures (kPa)
76.7	53.5
97.9	63.4
118.4	129.0
146.8	191.0

The purpose of this section is to propose a simple equation to predict the CT-B interfacial static pressures with respect to given wheel loading. The data in Table 2.3 can be normalized to develop an equation depending on the wheel loading. Corresponding to Figure 1.1, it can be said that only 21.93% of the wheel load appears directly below the wheel at the CT-B interface. The loads transferred to the CT-B interface are described as

"concentrated loads" in this current paper. The concentrated loads are shown in Table 2.4 and were calculated by multiplying the wheel loads by 0.2193.

Table 2.4 Load/Pressure distribution at the crosstie-ballast interface.

Wheel Loads (kN)	Concentrated Loads (kN)
76.7	16.83
97.9	21.46
118.4	25.97
146.8	32.19

If a linear trend line were drawn to determine the behavior of the measured data, the pressures would go to the negative magnitude at the wheel load of 0 kN. This is because the (0.001,0) point has been added to Table 2.4 to develop a power function. Hence, the equation to predict static contact pressures will be:

$$\sigma_s = 0.08679 \cdot (P_s \cdot \alpha)^{2.219} \tag{3}$$

where σ_s is the static pressure (kPa); P_s is the static wheel load (kN); α is the load distribution factor determined from Figure 1.1 as 0.2193.

The vertical stress at any depth can be determined using the Ahlf (2003) equation shown in Equation 1. Figure 2.5 illustrates the comparison of the Ahlf (2003) static pressures to the projected static pressures.

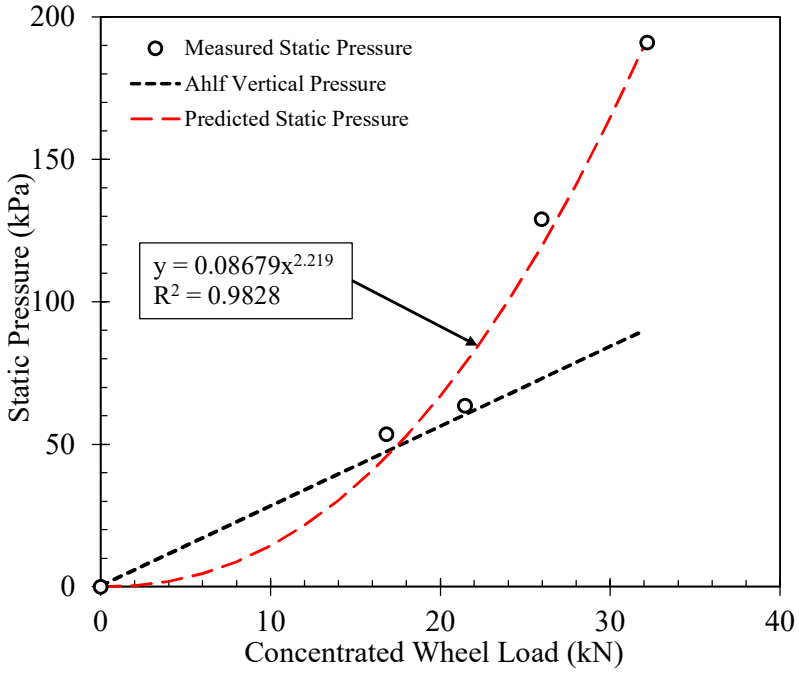

Figure 2.5 The comparison of the measured stresses and the Ahlf (2003) stresses and the function of predicted static pressures.

The pressures calculated using the Ahlf (2003) method are very similar to measured static pressures at lower wheel loads. However, once the method is applied to higher wheel loads, the difference between the two methods becomes more distinguishable. Additionally, the slope of the projected static pressures corresponding to the measured dynamic pressures tends to drop faster than that of the Ahlf (2003) vertical pressures. Concisely, the Ahlf (2003) method is more impractical in predicting a similar trend compared to the trend of the measured pressures. Therefore, a power function (Equation 3) was developed to predict static contact pressures at the CT-B interface at any given wheel load since the trends of the static pressures appear in the form of power functions.

2.3.2 Predicting the Dynamic Contact Pressures

The static contact pressures can be determined using Equation 3. The dynamic contact pressures can be predicted using the relationship between the static contact

pressures and the speed. This section will analyze the effect of speed, and a relationship will be found between static pressures and speed.

During the run-through tests, the dynamic contact pressures are highest at 64 km/h. Each pressure measured at each speed should be normalized to determine the effect of speed. The data was normalized by determining the ratios of dynamic pressures to static pressures, and Table 2.5 shows those pressure ratios at different speeds and wheel loads.

Table 2.5 The ratio of dynamic pressures to static pressures.

Wheel Loads (kN)	Speed (km/h)				
	3.2	16.1	32.2	48.3	64.4
	The ratio of dynamic pressure to static pressure				
76.7	0.97	0.95	0.89	0.92	0.73
97.9	0.98	0.96	0.99	0.92	0.86
118.4	0.98	0.97	0.98	0.95	0.87
146.8	0.99	0.96	0.94	0.91	0.85

Table 2.5 shows that speed has a slight effect on the pressures. As the trend of this effect has been analyzed, a relation can be developed between static pressures and dynamic pressures in terms of speed. Different wheel loads were executed by proportioning the dynamic pressures and static pressures. Figure 2.6 illustrates the ratio of dynamic pressures to static pressures at different speeds.

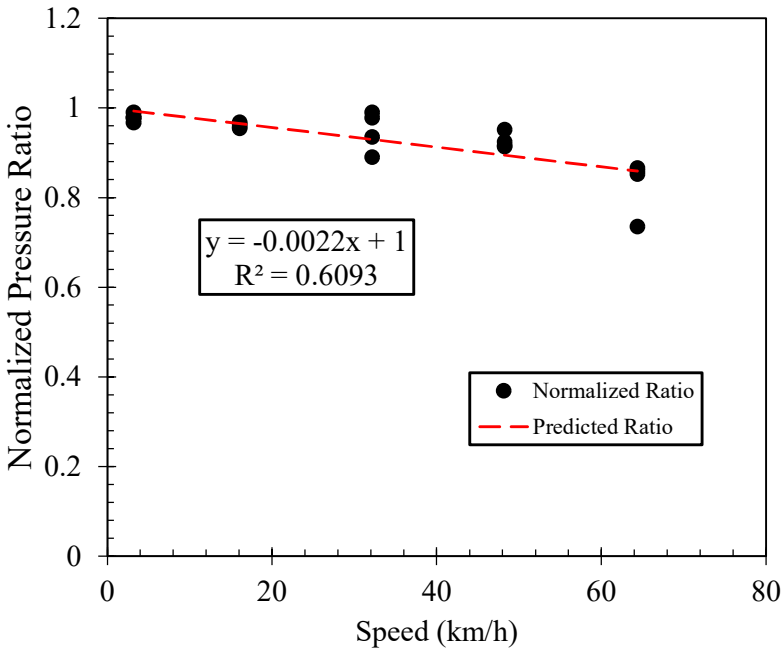

Figure 2.6 The normalized points at five different speeds.

The normalized points have a linear trend which is decreasing slightly. More particularly, the speed has a minimum effect on the ratio. The linear trendline shown in red in Figure 2.6 represents the predicted ratios. The equation for the predicted ratios can be described as:

$$\sigma_d = (m_1 V + 1) \cdot \left[0.08679 \cdot (P_s \cdot \alpha)^{2.219} \right] \tag{4}$$

where σ_d is dynamic pressure; P_s is the static wheel load (kN); α is the load distribution factor determined from Figure 1.1 as 0.2193; V is the speed of the train in km/h; m_1 is the slope of the trendline, which is -0.0022.

If the equation is simplified, the final expression of the equation will be:

$$\sigma_d = \sigma_s \cdot (-0.0022V + 1) \tag{5}$$

An error margin will appear since trendlines are used in the equations rather than exact measured stress magnitudes. The predicted and measured pressures are compared to show how the equations perform. Figure 2.7 illustrates the comparison between the predicted and the measured CT-B interfacial dynamic pressures. Red points represent the predicted pressures by using Equation 5.

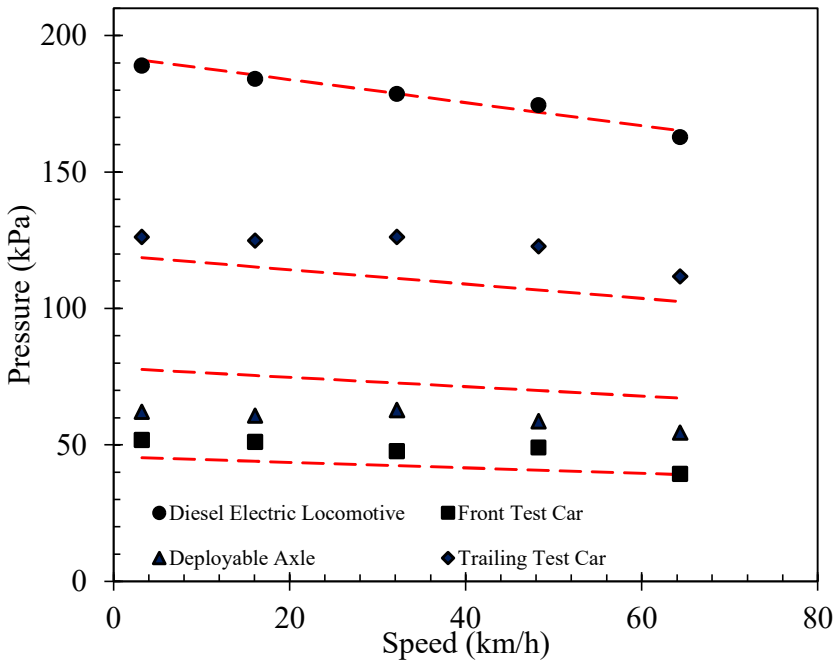

Figure 2.7 The comparison of predicted and measured dynamic pressures.

It is noted that the predictions of the dynamic contact stresses are more applicable at greater wheel loads compared to lower wheel loads. However, the magnitude differences between the predictions using Equation 5 and the measured pressures are neglectable compared to other methods [e.g., Talbot (1940) and Ahlf (2003)]. Table 2.6 shows the ratio of measured pressures to the magnitude difference between the measured and predicted pressures.

Table 2.6 The difference between measured and predicted dynamic pressures.

Wheel Loads (kN)	Speed (km/h)				
	3.2	16.1	32.2	48.3	64.4
	Error difference (%)				
76.7	-12.4	-13.8	-10.9	-16.7	-0.4
97.9	25.2	24.4	15.8	19.3	23.3
118.4	6.0	7.7	12.0	13.0	8.2
146.8	1.1	0.8	0.1	-1.4	1.5

Greater error margin percentages appear once two low magnitudes are proportioned to each other since the lower wheel loadings produce lower pressures. The program algorithm performs more efficiently at greater wheel loads, the most representative wheel load in ordinary traffic conditions. Figure 2.8 shows the error margin in percentage at various speeds and wheel loads.

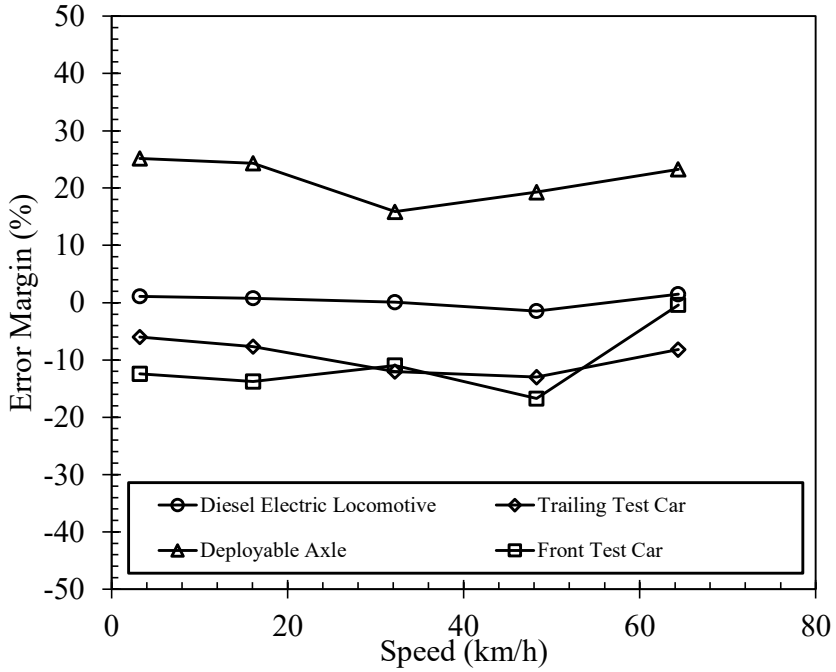

Figure 2.8 Error margin at various speeds of various wheel loads.

The greatest pressure determined using the presented equations is around 191 kPa, while the measured pressure is nearly 189 kPa. However, AREMA (2018) recommends 448 kPa as a maximum value for wood crossties. It is noticeable that AREMA design recommendations (2018) of the CT-B interfacial pressures are significantly overestimated. Therefore, the design recommendations might be reconsidered. The Talbot (1940) and Ahlf (2003) methods will be compared to square wave theory magnitudes in detail later in this current paper.

2.3.3 Square Wave Method Development

The assumption of the equal load distribution on the wheels is valid for this paper. Since loads are assumed to be distributed equally, the square waves can be used to present the pressures. More specifically, the pressures will be represented by "amplitudes," and the beginning of the wave will be described as the raising edge point. The ending of the wave will be described as the falling edge point, which is the point pressures reach 0 kPa. It will be repeatable for each bogie of the train set.

The maximum pressure will be experienced on the pressure cell directly below the wheel loading. However, the pressures do not appear suddenly. The magnitude of the pressure is compounding as the wheel approaches the pressure cell. The fundamental problem is that the distribution of the affected area due to dynamic wheel loads is uncertain. This section discusses the development of the square wave method to predict dynamic contact pressures at the CT-B interface based on basic inputs such as the weight of the train, speed, and the distance between wheels.

The impact loadings were normally minimal for the FRA test trains since the wheels were maintained to minimize imperfections. However, the data must have been filtered since some produced pressure values were in excess of nominal pressure values. The time increment was 0.0005 seconds for the collected data. Since the time increment was very small, the pressures varied widely, inducing sharp changes along pressures. Therefore, the data should be filtered in order to have smoother values.

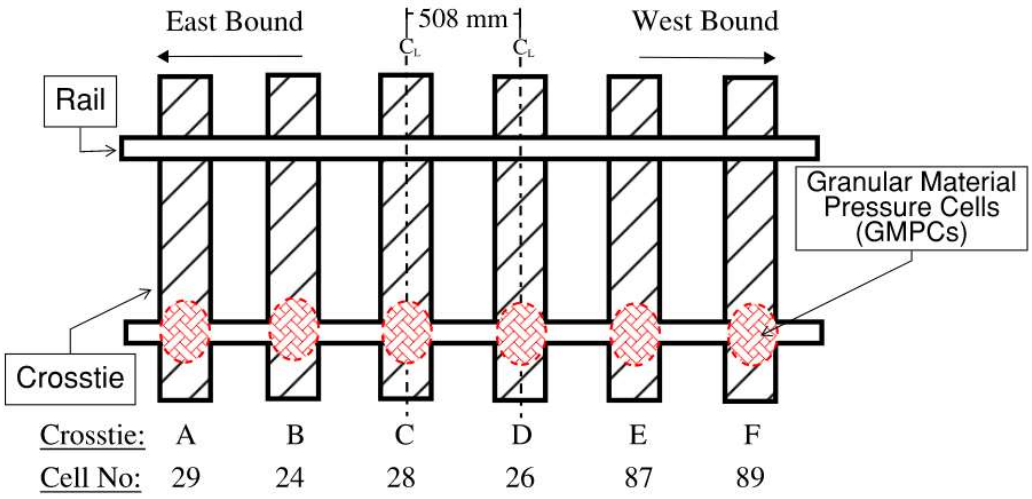

Figure 2.9 Granular Material Pressure Cell layout at the test site.

The data was recorded in the time domain. However, it is often desired to perform a Fourier transform to view the data in the frequency domain. The sampling rate can be described as the number of samples acquired per second. Specifically, the sample rate is the ratio of 1 to time increment. The data was processed with the Signal Processing Toolbox of MATLAB R2021b (2021). Since the time increment was 0.0005 s for the data collected, the sample rate was used as 2000/sec in order to represent the signal strength. The most dominant frequencies were at 80 Hz based on the spectrogram. Therefore, new peaks were estimated at 80 Hz. Since the more representative data points were produced, it is possible

to develop the affected distance functions from estimated peaks, the beginning and ending points of pressures. Cell 89 at the interface of the Crosstie F and ballast was considered a reference cell pressure during the analysis process. Figure 2.9 shows the GMPCs layout at the test site.

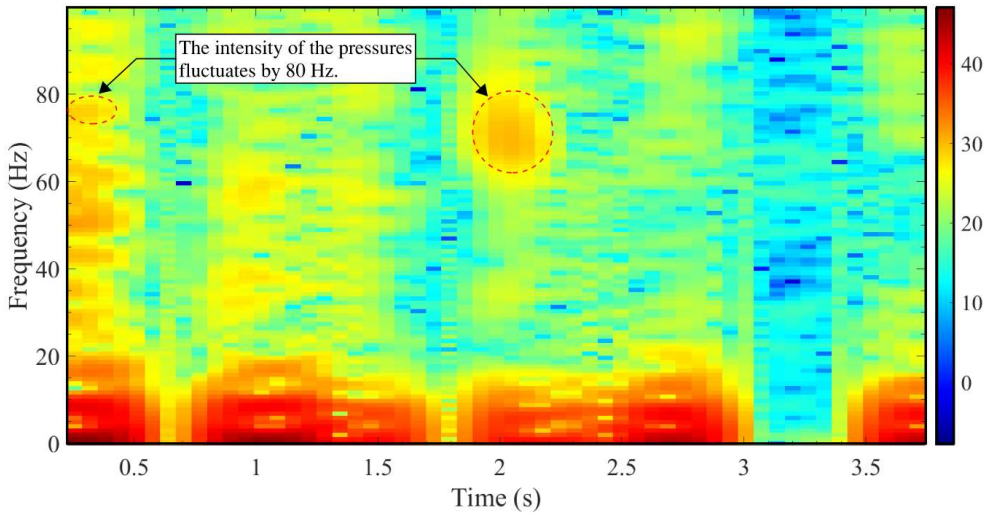

Figure 2.10 The image of the spectrogram.

The most dominant frequency was 80 Hz based on the spectrogram. If a higher frequency than 80 Hz was selected to develop a bandwidth filter, the low magnitude peak pressures might have escaped notice, such as the peak pressures for DOTX 218 test car. If a smaller frequency than 80 Hz was selected, the peak pressures might have been undetermined. This is because a bandwidth filter was developed at 80 Hz to determine the MATLAB estimated peaks. The script for bandwidth filtering is shown in Appendix C. Figure 2.10 shows that the image of the spectrogram.

Figure 2.11 illustrates the predicted peak points using the MATLAB bandwidth filtering tool. The red waves represent the predicted pressure waves, while the blue ones are the original data.

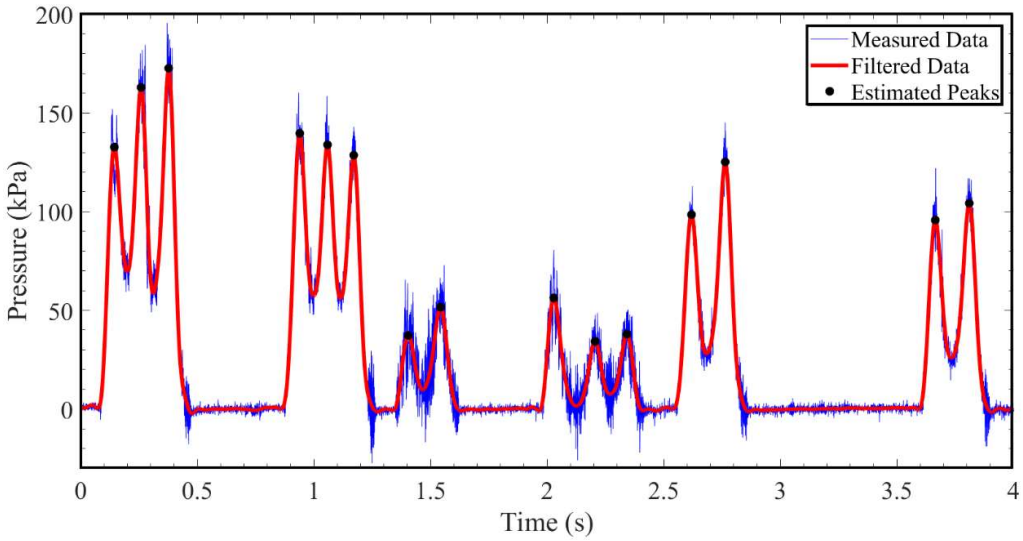

Figure 2.11 Predicted pressure waves of Cell 89 with peak points at 80 Hz.

The points that the pressure cells started sensing pressures were predicted to develop a function based on speed and wheel loads by filtering the raw data. The peak pressures were predicted for each pressure cell, and the peaks were averaged in order to see the performance of the square wave theory. The peak pressures of the reference cell were replaced by the average peak pressure magnitudes of six consecutive cells. Since the distances between wheels are known and the times were found after the filtering process, the actual speed of the trucks can be determined. Subsequently, the actual speeds were calculated to determine the affected distances. The affected dynamic distances at each speed of each car were determined by using this square wave theory.

This information makes it possible to develop a function for affected distance due to wheel load and speed. However, there will be four different affected distances due to the dynamic wheel load, and they will be expressed as a, b, c, and d, respectively. Figure 2.12 represents the a, b, c, and d distances.

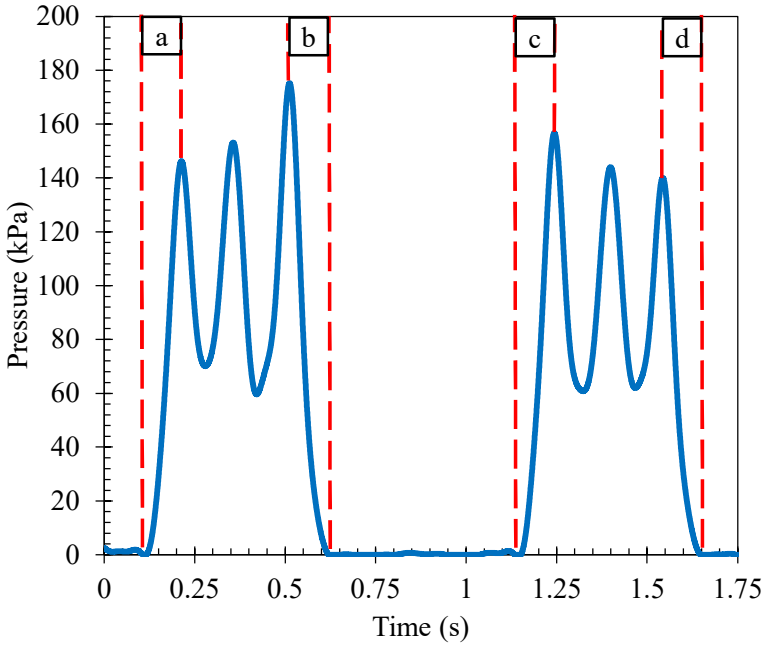

Figure 2.12 The demonstration of the a, b, c, and d distances.

The affected distances shown in Figure 2.12 were determined using the Mathcad Prime 7.0 (2021) software. An example calculation sheet is shown in Appendix D. Figure 2.13 shows the affected distances at different speeds and is limited to three different wheel loads.

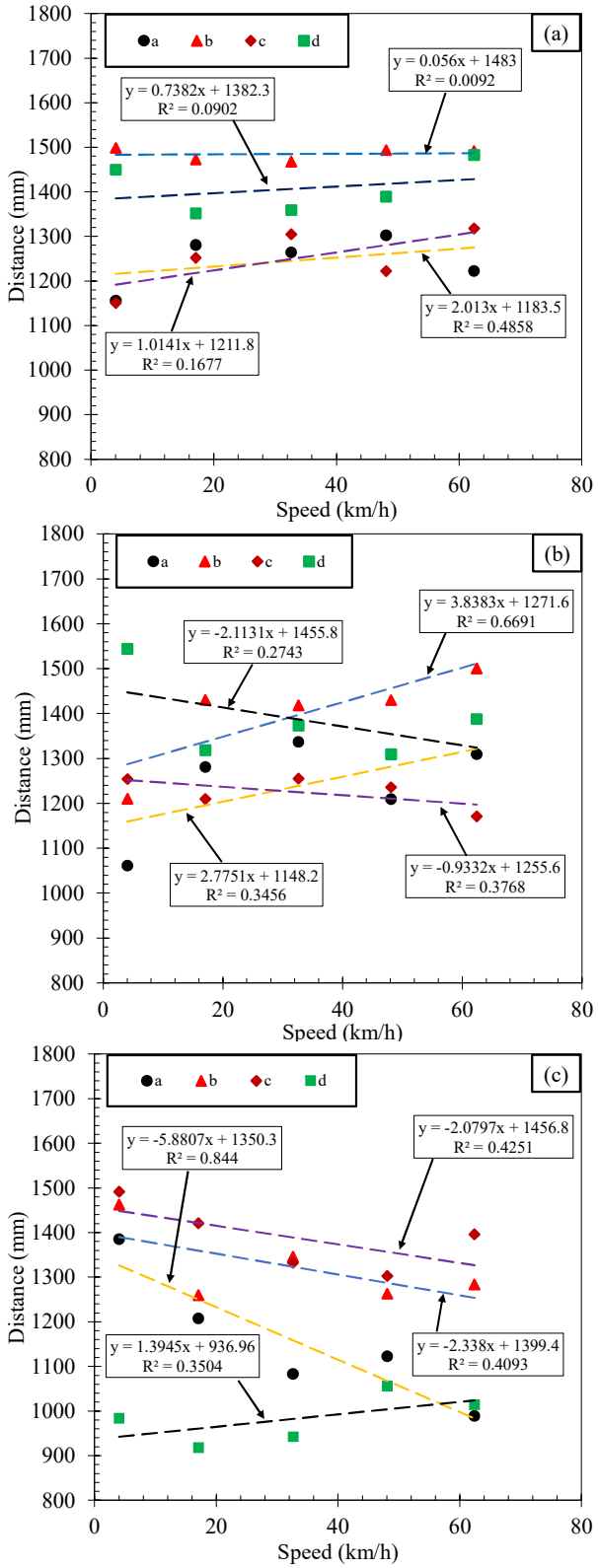

Figure 2.13 (a) The affected distance at different speeds for 146.8 kN; (b) The affected distance at different speeds for 118.4 kN; and (c) The affected distance at different speeds for 76.7 kN.

The intercepts of the trendlines of the figures above illustrate the affected static distances. Table 2.7 shows the static distances at various wheel loads. This theory cannot be applied to the deployable axle since the deployable axle is a single axle, and the calculations do not include the wheel load of 97.9 kN.

Table 2.7 Static affected distances at different speeds for different wheel loads.

Wheel Loads (kN)	Concentrated Loads (kN)	a (mm)	b (mm)	c (mm)	d (mm)
76.7	16.83	1211.8	1483	1183.5	1382.3
118.4	25.97	1148.2	1271.6	1255.6	1455.8
146.8	32.19	1350.3	1399.4	1456.8	936.96

Figure 2.14 shows the trends of static affected distances based on the concentrated wheel loads.

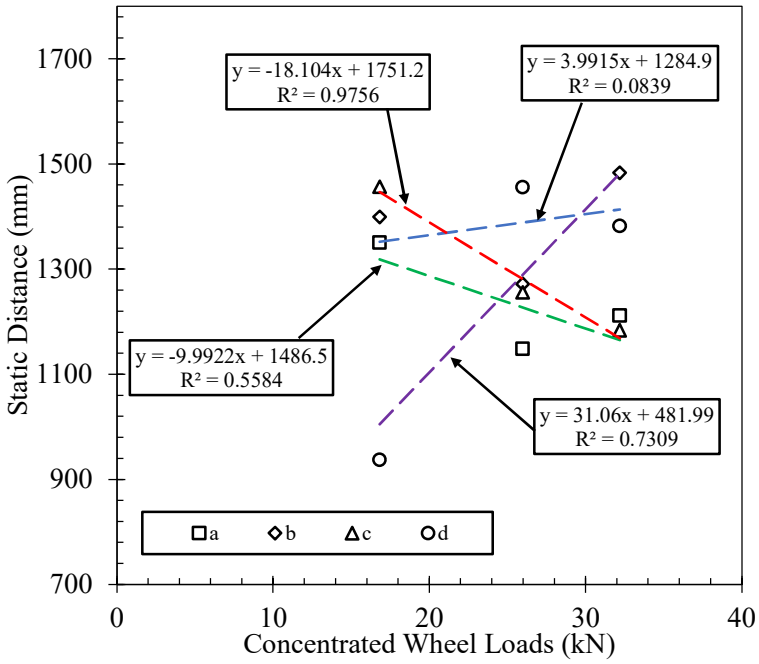

Figure 2.14 The trends of static distances based on concentrated wheel loads.

The static distance for any wheel load can be calculated by the linear regression of the data in the form of Equation 2, where y is the static distance (mm); x is the concentrated wheel load (kN); m is the slope of the line; b is the intercept. Table 2.8 present the coefficients of the linear equations to predict the static distance based on wheel loadings. The R-squared values are low since the analysis process was limited to three different wheel loadings. However, it is important to note that the affected distance functions are for only visual purposes.

Table 2.8 The coefficients of the linear equations to predict the static distance due to wheel loadings.

Static Distance (mm)	Slope	Intercept
a_s	-9.9922	1,486.5
b_s	3.9915	1,284.9
c_s	-18.104	1,751.2
d_s	31.06	481.99

The data was normalized with the ratio of the dynamic affected distance to static affected distance. Thus, the effect of the speed can be determined. Figure 2.15 shows that the speed slightly affects the affected distances.

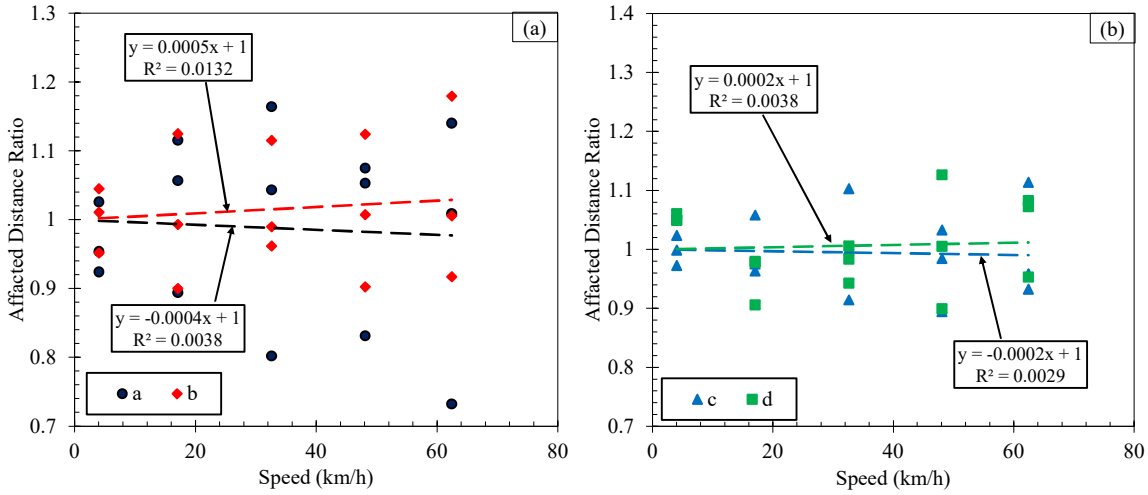

Figure 2.15 (a) The effect of the speed on the distances for a and b sides; (b) The effect of the speed on the distances for c and d sides.

The following equations based on speeds for the a, b, c, and d sides are expressed by the linear regression of the data in the form of Equation 2, where y is the static distance ratio; x is the speed (km/h); m is the slope of the line; b is the intercept. Table 2.9 presents the coefficients of the linear equations to predict the static distance based on wheel loadings.

Table 2.9 The coefficients of the linear equations to predict the static distance ratios based on speed.

Static Distance Ratio	Slope	Intercept
a_r	-0.0004	1
b_r	0.0005	1
c_r	-0.0002	1
d_r	0.0002	1

Since both the static affected distances and the ratios for each affected side can be calculated, the dynamic affected distance can be calculated as:

$$D_d = D_s \cdot R \qquad (6)$$

where D_d is the dynamic affected distance in mm; D_s is the static affected distance in mm; R is the ratio of the dynamic affected distance to the static affected distance.

The distances between wheels are known, and the affected distances can be calculated using Equation 6. The theory shown in Figure 2.12 can be used to determine the width of the square, which can be expressed as the length of the truck. Thus, the width of the square wave for the six axles locomotive will be:

$$L_1 = D_{12} + D_{23} + a + b \tag{7.1}$$

$$L_2 = D_{45} + D_{56} + c + d \tag{7.2}$$

where L_1 is the length of the first bogie (mm); L_2 is the length of the second bogie (mm); D_{12} is the distance between the first wheel and second wheel (mm); D_{23} is the distance between the second wheel and third wheel (mm); D_{45} is the distance between the fourth wheel and fifth wheel (mm); D_{56} is the distance between the fifth wheel and sixth wheel (mm).

The same theory is applied to the cars as well. The car wheel order will change since a regular car has four axles. On the other hand, the theory shown in Figure 2.12 can be used to determine the distance between trucks and between locomotives and cars. The distance between trucks is expressed as:

$$L_t = D_{34} - b - c \tag{7.3}$$

where L_t is the distance between trucks (mm); D_{34} is the distance between the third wheel and fourth wheel (mm).

The ordinal number of the last wheel of each truck may vary according to the locomotive design or cars. Essentially, the theory can be explained as b and c distances are subtracted from the distance between the last wheel of the front truck and the first wheel of the trailing truck. The same theory can also be applied to determine the distance between locomotives or cars. However, the coupler lengths should be added to the distance from the center of the last wheel of the front vehicle to the back of the vehicle frame and that of the first wheel of the trailing vehicle to the head of the vehicle frame.

$$L_c = (L_b + L_f + L_{fc} + L_{bc}) - a - d \tag{7.4}$$

where L_c is the distance between cars or locomotives (mm); L_b is the distance from the center of the last wheel to the end of the vehicle frame of the front vehicle (mm); L_f is the distance from the center of the first wheel to front (head) of the vehicle frame of the trailing vehicle (mm); L_{fc} is the length of the front coupler of the trailing vehicle (mm); L_{bc} is the length of the back coupler of the front vehicle (mm).

Amplitudes and the width of the pulses are used to develop a square wave function. Amplitude represents the CT-B interfacial dynamic pressures, while the width of the pulse represents the length of the bogies, the distance between bogies, and the distance between vehicles. An algorithm can be developed to predict dynamic contact pressures at the CT-B interface for an unlimited number of trains with basic information by using the presented square wave theory.

2.3.4 The Flow Chart of the Square Wave Theory Algorithm

An algorithm was developed by using the square wave theory to predict pressures. The algorithm was written in Python 3.0, and the script of the algorithm is shown in Appendix E. Firstly, inputs (e.g., train speed, the weight of the train, distances between wheels, and so on) are required by the user. Subsequently, wheel loads and distances to predict affected distances can be calculated by using the desired operating information. Since Microsoft Excel is a common platform with a simple user interface, an Excel input file was created. The Excel file asks the user to provide the basic information. A table that describes the Excel Input file is shown in Appendix F. After the user gives the information required, the algorithm will compute the Excel input and predict the dynamic contact pressures based on the provided information. The algorithm is illustrated by the flowchart in Figure 2.16:

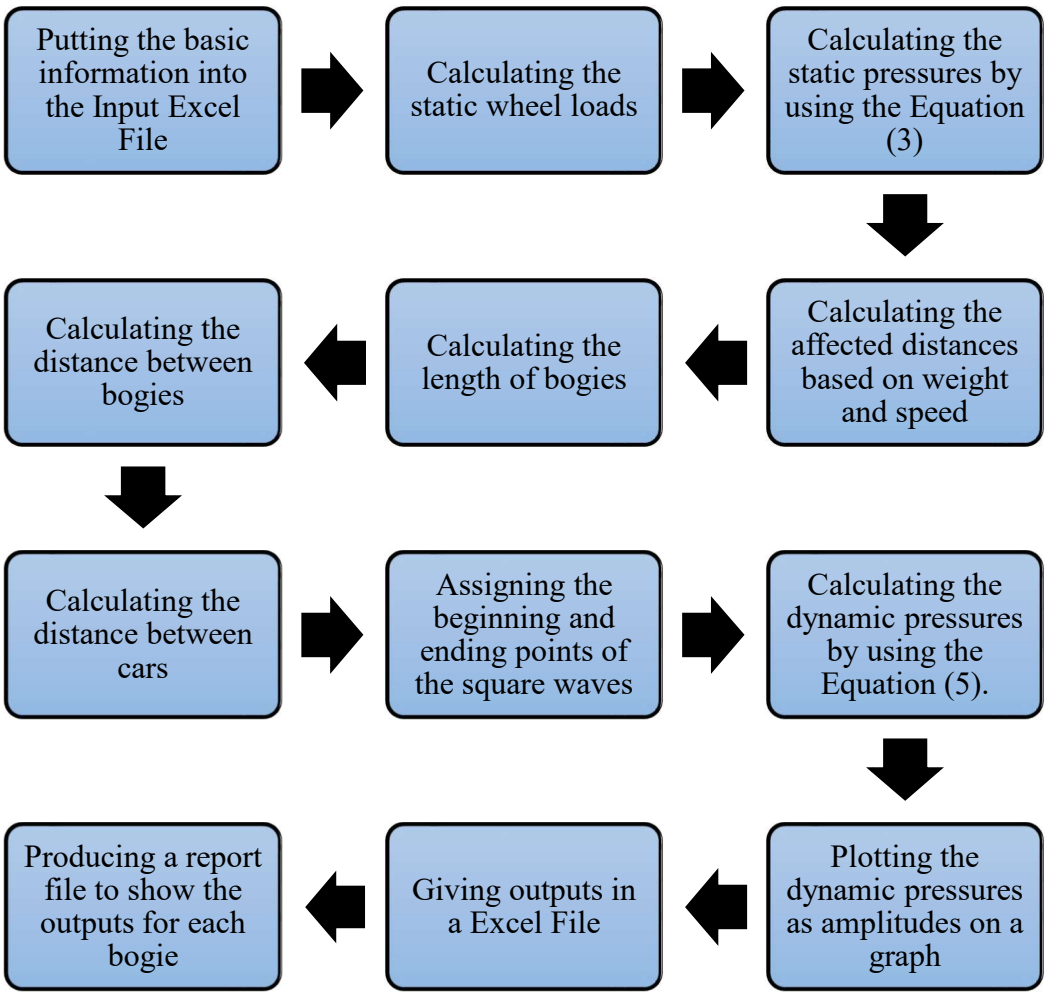

Figure 2.16 The flowchart of the algorithm of the square wave theory.

An example with three locomotives and four cars is provided to depict how the algorithm works. The total weights of each locomotive and car differ to display the pressure variance. The operation speed was 50 km/h for this example illustration. The input weight values are shown in Table 2.10.

Table 2.10 Input vehicle weight values for each locomotive and car.

Car Type	Car Order	Vehicle Weight (kN)
Locomotive	1	1735
Locomotive	2	1690
Locomotive	3	1646
Car	4	948
Car	5	979
Car	6	890
Car	7	800

The pressure-time graph is given as output after the algorithm is executed. Figure 2.17 shows the output plot of this example.

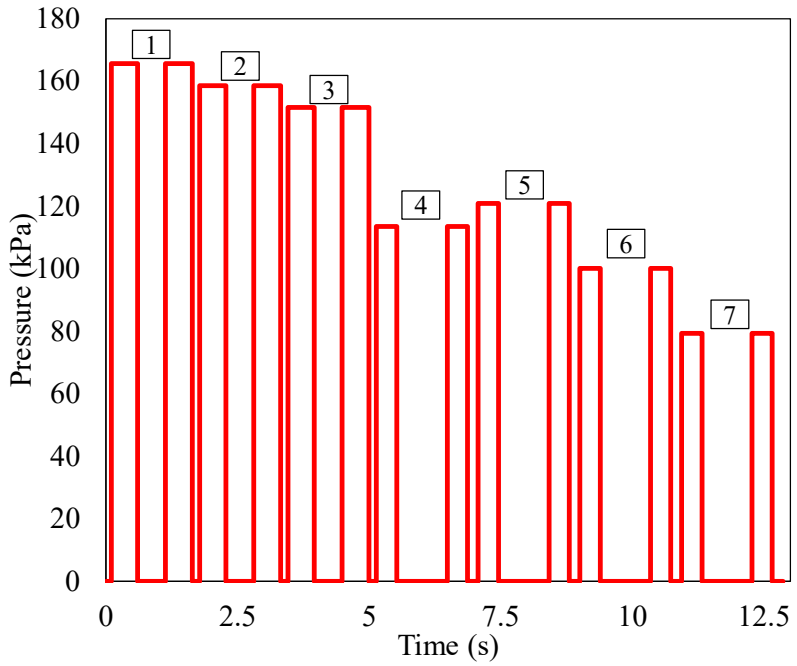

Figure 2.17 The output plot of the algorithm of square wave theory.

2.4 DATA MATCHING

The output of the algorithm and in-track test pressure waves were compared to confirm the productivity of the square wave theory. Figure 2.18 shows the comparison of

the predicted dynamic pressures and the in-track test pressures for the diesel-electric locomotive at 64 km/h, while Figure 2.19 illustrates the comparison of the predicted dynamic pressures and the in-track test pressures for the inspection car at 48 km/h.

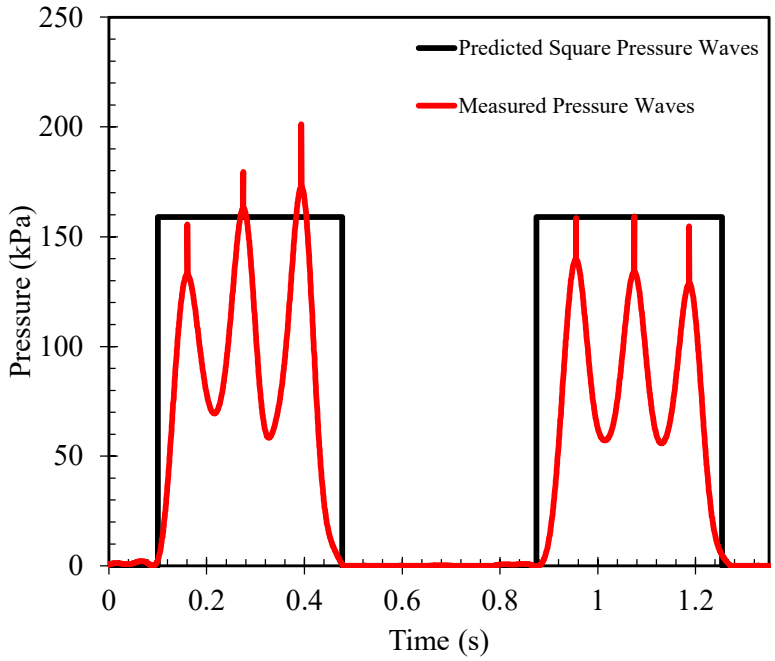

Figure 2.18 The predicted dynamic pressures at 64 km/h for the diesel-electric locomotive using the square wave theory.

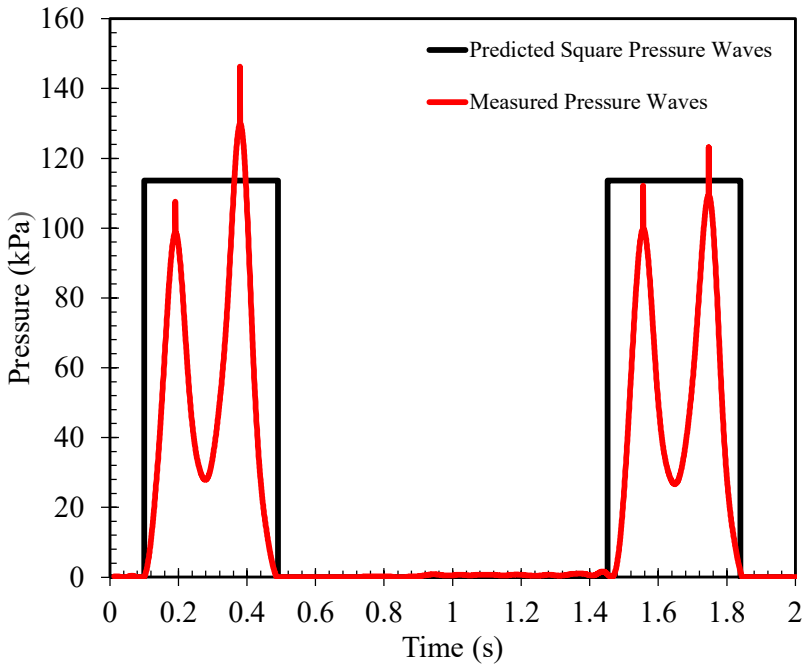

Figure 2.19 The predicted dynamic pressures at 48 km/h for the inspection car using the square wave theory.

Figure 2.18 and Figure 2.19 shows the square wave theory algorithm is performing productively to predict the average peak pressures. Since Cell 89 was used as a reference cell and the peak pressure of the reference cell was lower than the average peak pressures, the average peak pressures of the six cells were replaced with the peak pressures of the reference cell. Hence the apex portion of the red waves does not look smooth. The y-axis corresponds to pressures (kPa), and the x-axis corresponds to time (s). The red lines illustrate the measured average pressures, and the black waves show the predicted square waves.

2.5 CONCLUSIONS

In this study, it was concluded that the CT-B interfacial dynamic contact pressures have been overestimated for many years. The design recommended practices based on the

Talbot (1940) methodology are no longer valid for modern-day railroad infrastructure and rolling stock. There are multiple reasons, such as the sensitivity and reliability of the measurement devices used for traditional equations, inconsistent supporting conditions during the testing process, increased axle loads, different track designs (asphalt), transition to continuous welded rails, and others. Therefore, a new method was developed to predict the dynamic 41ebastiaes at the CT-B interface using basic information provided by revenue trains. An advanced measurement device for railroad ballast was used to measure the real-time dynamic pressures at the CT-B interface. The tests were conducted using FRA Test Trains (NS SD60E Diesel-Electric Locomotive, DOTX 218 Test Car, and DOTX 220 Inspection Car) in Mascot, TN in 2018. The tests were conducted at a maximum train speed of 64 km/h. Impact loading was minimal for test vehicles since the wheels and trackbed were well maintained. The measured data was analyzed to propose multiple equations.

This research shows that calculated results by the Ahlf (2003) method do not increase as rapidly as the measured data, in particular at higher wheel loads. This is because a new equation was proposed to predict "static pressures" at the CT-B interface (see Figure 2.5).

The traditional Talbot (1940) equation assumes that dynamic contact stresses increase with speed. However, this research does not support those assumptions. The speed increasing has a minimum effect on measured dynamic pressures, and the pressures slightly decrease with increasing speed. It is important to note that the train speed used during the testing process was limited to a maximum of 64 km/h. Therefore, another equation was proposed to predict the dynamic contact pressures at the CT-B interface. The predictions for the dynamic contact pressures are more representative at higher wheel loads compared

to the lower wheel loads. However, the predictions are still performing more adequately than the traditional Talbot (1940) method.

Additionally, combined equations were proposed to determine the affected distances due to the dynamic wheel loads. By calculating the affected distance, the square wave theory can be used to predict pressures for each truck of the train. However, the affected distance equations are more suitable for visual purposes. A square wave algorithm was developed to combine these three main equations and predict dynamic pressures at the CT-B interface for any given number of trains using basic information such as train speed, weight, and wheel distances.

2.6 ACKNOWLEDGEMENTS

This research was primarily funded by the National University Rail Center (NURail). A special thanks to prior Graduate Assistants Ethan Russell and Travis J. Watts, Visiting Scholar Qinglie Liu, and Prof. David B. Clarke for their significant contributions during the early phases of this research. The cooperation and contributions of Norfolk Southern Corporation during the test site installation activities and continued monitoring activities are greatly appreciated. I also acknowledge this contribution to this research by Federal Railroad Administration Office of Research Development and Technology, ENSCO Inc., and the Volpe National Transportation Systems Center. A special thanks to Huseyin Cinar for his significant contribution on the program coding.

THE ANALYSIS OF STRESS DISTRIBUTION IN THE RAILROAD TRACK STRUCTURE

ABSTRACT

Excessive crosstie wear and abrasion and ballast wear and fouling are fundamental problems contributing to inadequate railroad track performance. This adversely affects the attainment and long-term maintenance of desired track geometric requirements. The magnitudes and distribution of the stresses at the crosstie-ballast (CT-B) interface must be known to determine the stress distribution on and within the ballast. However, the stresses at the top of the ballast often vary significantly. This study provides a successful method to measure the dynamic contact stresses at the interface of CT-B by a research test train using granular material pressure cells. A data set of CT-B interfacial pressures, taken from a freight mainline in Mascot, TN, in 2018, was analyzed to better understand stress distribution through the railroad trackbed. Additionally, the obtained data were compared to traditional recommended design practices and the developed square wave theory. A Gaussian stress distribution equation was developed to determine longitudinal stress distribution over the crossties for static conditions. Also, the stress distribution along the crossties is presented. Based on the analyzed CT-B interfacial pressures, the ballast stress distribution is discussed, and recommendations are made.

KEYWORDS: Trackbed Pressure measurement, crosstie, Gaussian stress distribution, railroad, stress distribution, ballast

3 THE ANALYSIS OF STRESS DISTRIBUTION IN THE RAILROAD TRACK STRUCTURE

3.1 INTRODUCTION

Railroad trackbed design is essential to sustain loading stresses acting on the track structure (Indraratna and Ngo 2018). The fundamental elements of a railroad track can be described as the rail, crosstie, ballast, sub-ballast, and subgrade. Figure 3.1 shows the cross-section of railroad track elements. Wheel loading pressures are transferred through these elements with diminishing intensities.

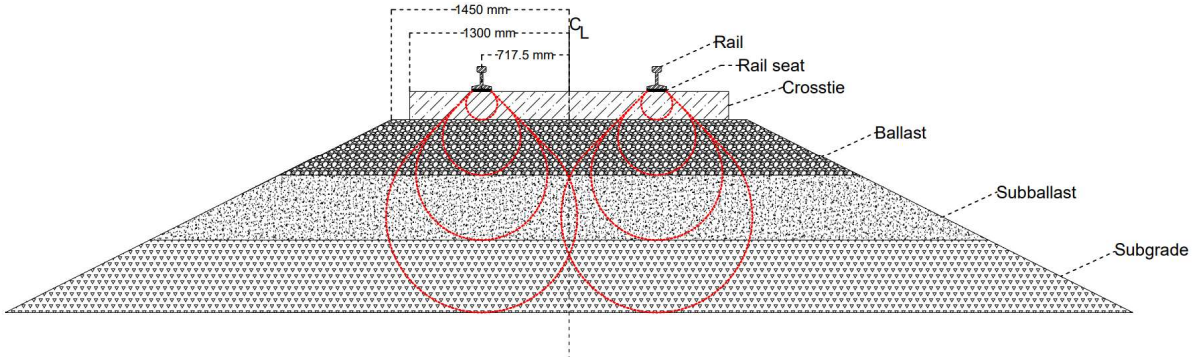

Figure 3.1 The fundamental elements of railroad track and support.

Pressures on the components of railroad infrastructure are primarily functions of the static loads, train speed, layer quality and dynamic loading factors. The red curves in Figure 3.1 represent the pressure distribution along the railroad track components. The crosstie is exposed to the greatest pressure, and the subgrade experiences the least pressure since pressure loss occurs at each interface. Greater wheel loadings produce higher pressures through the ballast. Additionally, with the increased transportation demand, train speeds and axle loads increase remarkably, and various degrees of settling or other track problems may occur due to high pressures transferred to the railroad track (Wang et al.

2020). Therefore, determining pressures within the railroad track is paramount for inclusion in design practices to prevent inadequate track performance, such as crosstie wear and abrasion and ballast wear and fouling.

The American Railway Engineering and Maintenance-of-Way Association (AREMA) is the leading railroad industry authority and publishes recommended trackbed design practices in the United States of America (AREMA, 2018). The recommendations for trackbed are largely based on the Talbot (1940) methodology, which was outlined in the seven progress reports of the American Railway Engineering Association (AREA) between 1918 and 1940 (AREA 1980). The analysis presented in the initial progress report (Talbot 1918) was based on data collected from various pressure capsules measuring trackbed pressure and elastic deflection. These pressure capsules measured the elastic deflection using a micrometer placed in the center of a hardened steel diaphragm. The micrometer reading was converted to a pressure measurement using the material properties. However, Watts and Rose (2018) state that these measurement devices were not sufficiently sensitive to accurately determine the pressures in the railroad track.

The Talbot (1919) method used the relationship between flexural curves of the crossties and the bending moment to determine stress distributions. Higher stresses occur as bending moments increase. However, the Talbot (1919) method also determined the stresses are functions of the crosstie supporting conditions. If the ballast supporting conditions are not uniform along the crosstie, additional bending stresses develop where the crosstie experiences less or decreased quality support. Although Talbot (1940) later found a means to place the pressure capsule device at the crosstie-ballast (CT-B) interface precisely, direct measurements were inconsistent (Watts and Rose 2018). Talbot (1919)

assumed that the load distribution along the crosstie is uniform, with the outer two-thirds of the crosstie distributing the loads (Hay 1982). However, this assumption may be invalid since Talbot (1919) had inconsistent supporting conditions when measuring the stresses in the railroad track during the study.

Additionally, jointed rails were used in the early 1900s during the in-track testing program (Talbot 1919); as the wheels 'jumps' the rail joint gap, this generates significant impact dynamic conditions. Later, beginning in the 1930s, continuous welded rails began to replace jointed rails. It is currently used exclusively by the US railroads for high tonnage mainlines. Over 130,000 kilometers of main track in the US had continuous welded rail by 1980 (Abbey 1985).

Wheel and rail irregularities may also contribute to inconsistency in the Talbot (1919) measurement data. Although it was possible to distinguish the effects of rail and wheel irregularities during the study, lower accuracy compared to current laser measurement technology limited the utility of the rail and wheel irregularity measurements. These irregularities significantly contribute to the impact pressures exhibited at the CT-B interface. Today the widespread adoption of Wheel Impact Load Detectors (WILDs) provides a means to monitor wheel-tread/rail surface irregularities for revenue trains; defective wheels are replaced with new wheel sets.

Advanced methods have been developed since the Talbot (1919) study to measure railroad track pressures using hydraulic pressure sensors. Hydraulic pressure sensors (transducers) use fluid dynamics to measure pressure. Fluctuation in the hydraulic fluid pressure is converted into electric signals expressing pressure measurements. Therefore, more reliable and sensitive measurement data can be obtained.

This paper presents an advanced method to measure dynamic contact pressures at the CT-B interface. This is compared to the recommended practice (Talbot 1940) method, the Ahlf (2003) method, and the square wave theory (Unluoglu et. 2022) using measured data from Federal Railroad Administration (FRA) research test trains. Commonly used assumptions in the railroad industry are discussed, and recommendations are made based on results and analyses.

3.2 DATA ACQUISITION

High-quality railroad track designs are cost-effective and easily maintained. Quantifying CT-B interface stress distributions may be considered helpful in optimizing design practices for achieving a high-quality track. Hydraulic earth pressure cells (EPCs) were used in this study and are designed to measure pressure changes in granular materials such as railroad ballast. EPCs were composed of two stainless steel, 230 mm cylindrical disks filled with hydraulic fluid welded together at their periphery. The pressure transducer had a 1.5 factor of safety; having an extra factor of safety is quite helpful for this research since wheel impacts may notably occur in high-pressure increases (Geokon 2017).

The EPCs were placed at the CT-B interface along six consecutive wood crossties on an active track. The study used a procedure to limit changes in the existing ballast conditions during the placement of the EPCs. Mild disturbance of the ballast during the installation of the instrumented crossties required surfacing and tamping to achieve the desired ballast compaction, consistent support, and track geometry in the site area (Rose et al. 2018). Figure 3.2 represents the configuration of the EPCs in the railroad track.

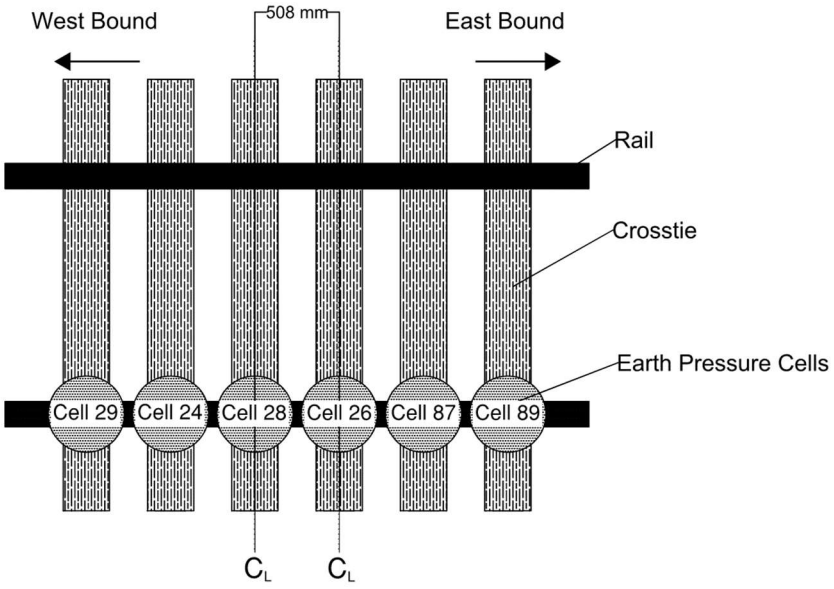

Figure 3.2 The trackbed pressure test configurations of earth pressure cells (after Russell et al. 2018).

FRA test trains were used in this study. The lead car was a 6-axle NS SD60E Locomotive with a wheel load of 148 kN, and the trailing car, DOTX 220, was the inspection car with a wheel load of 119 kN. It was assumed that the load distribution was equal on each wheel. The DOTX 218 test car had different wheel loads based on the deployable axle load. The deployable axle on the DOTX 218 test car had a wheel load of 98 kN, the remaining wheels had a wheel load of 77 kN, respectively, accounting for the remaining load distribution.

The train was operated from west to east along the track. Figure 3.3 illustrates the raw pressure data on the reference pressure cell (Cell 89) when the FRA test train operated at 64 km/h.

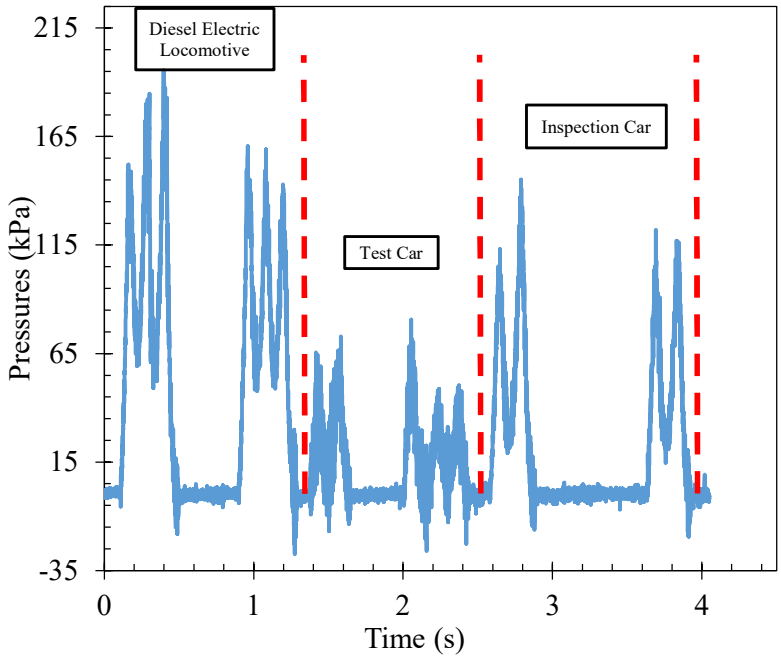

Figure 3.3 The raw pressure data on the reference pressure cell with 64 km/h train speed.

Note that the wheel impact loading was minimal for the test cars and locomotive since the wheels were regularly maintained to mitigate tread imperfections. The FRA test trains traversed a Wheel Impact Load Detector (WILD) installation at Ebenezer, TN, at a speed of 64 km/h just before conducting the pressure cell tests (Russell et al. 2020). WILD is an advanced data acquisition system that measures the actual conditions of the wheel (Stratman et al. 2007).

3.3 SITE LOCATION AND CONDITIONS

The test site was located on the Norfolk Southern (NS) mainline in Mascot, TN (Mile Post 117.3), just East of Knoxville, TN. The alignment was a tangent section with a 0.25 percent of the ascending grade to the East (Russell et al. 2020). The annual traffic on the line was approximately 33.6 million gross metric tons with a maximum speed of 72 km/h. Figure 3.4 shows the location of the test field.

Figure 3.4 Test site location.

High-grade railroad rail type 136 RE continuous welded rail was in use on the track with cut spike fasteners to wood crossties. The crossties were spaced 508 mm from center-to-center, and each crosstie was box anchored. Track support consisted of standard NS mainline granite ballast on a well-supported rail line (Russell et al. 2020). The ballast was well drained and clean; no ballast fouling or mud was indicated in the test area. NS personnel reported that the track was generally stable and required minimum maintenance. The wood crosstie track was timbered and surfaced two years before the installation of the instrumented crossties. Double tamping was performed upon placing the pressure cell devices to ensure that the instrumented and approach crossties were uniformly tamped to match existing conditions prior to instrument installation. This provided equivalent contact support across all concurrent and adjacent crossties. Lastly, the track was raised and tamped through the site area (Russell et al. 2020).

3.4 SPEED EFFECT TO CROSSTIE-BALLAST INTERFACE PRESSURES

The magnitudes of the CT-B interfacial pressures were unknown and the uncertainty of these pressures may affect the track design and performance. The stresses are functions of the dynamic loads applied on the track during train operation. Dynamic loads generally differ from the magnitude of static wheel loads (Li et al. 2016). A static load can be multiplied by a dynamic load factor to approximate a dynamic load. Specifically, the relationship between dynamic loads and static loads can be expressed with the dynamic load factor:

$$P_d = P_s \cdot \alpha \tag{8}$$

where P_d is the dynamic load (kN); P_s is the static load (kN); α is the dynamic load factor (Hay, 1982).

Recommendations differ for dynamic load factors. Doyle (1980) provides a list of dynamic wheel load factors and the corresponding mathematical expression with required variables, as shown in Table 3.1. Table 3.2 provides variable definitions of the dynamic load factors.

Table 3.1 Different types of dynamic load factors (Doyle 1980).

Dynamic Load Factor	Expression	Train Speed	Wheel Diameter	Static Wheel Load	Unsprung Mass	Vehicle Center of Gravity	Locomotive Maintenance Condition	Track Modulus	Track Stiffness at Rail Joint	Track Joint Dip Angle	Cant Deficiency in Curves	Curve Radius	Track Maintenance Conditions
Talbot	$1+\frac{33\cdot V}{100\cdot D}$	•	•										
Indian Railways	$1+\frac{V}{3\sqrt{U}}$	•						•					
Eisenmann	$1+\delta\cdot\eta\cdot t$	•											•
ORE/Birmann	$1+\alpha+\beta+\gamma$	•				•	•				•	•	•
German Railways	$1+\frac{11.655\cdot V^2}{10^5}-\frac{6.252\cdot V^3}{10^7}$	•											
British Railways	$1+14.136(\alpha_1+\alpha_2)\cdot V\cdot\sqrt{\frac{D_j\cdot P_U}{g}}$	•		•	•				•	•			
South African Railways	$1+0.312\cdot\frac{V}{D}$	•	•										
Clarke	$1+\frac{15\cdot V}{D\sqrt{U}}$	•	•					•					
WMATA	$(1+0.0001\cdot V^2)^{2/3}$	•											
Sadeghi	$1.098+0.00129\cdot V+2.59\cdot(10^{-6})\cdot V^2$	•											
AREMA C30	For $20<V<120$: $0.6+0.005\cdot V$	•											

Table 3.2 The definitions of variables (Doyle 1980).

Variable	Definition
V	Train speed (mph)
D	Wheel diameter (in)
U	Track modulus (psi)
δ	0.1, 0.2, 0.3 depending on track conditions
η	1 for vehicle speeds up to 37 mph $1 + \frac{V-37}{87}$ for vehicle speeds between 37 and 125 mph
t	0, 1, 2, 3 depending on chosen upper confidence limits defining probability of exceedance
α	Coefficient dependent on level of track, vehicle suspension, and vehicle speed, estimated to be $0.167 \cdot (\frac{V}{100})^3$ in most unfavorable case
β	Coefficient dependent on wheel load shift in curves (0 in tangent track)
γ	Coefficient dependent on vehicle speed, track age, possibility of hanging crossties, vehicle design, and locomotive maintenance conditions, estimated to be $0.10 + 0.071(\frac{V}{100})^3$ in most unfavorable case.
$\alpha_1 + \alpha_2$	Total rail joint dip angle (radians)
D_j	Track stiffness at the joints (kN/mm)
P_u	Unsprung weight at one wheel (kN)
g	Acceleration due to gravity (m/s^2)

The dynamic load factor is crucial in determining dynamic contact pressures at the CT-B interface. This research uses the Talbot dynamic load factor, which is still used in North American track analysis (Van Dyk et al. 2013). The Talbot (1940) method is commonly used to calculate the dynamic pressures (Hay 1982) and is expressed as:

$$P_a = \frac{2P}{\left(\frac{2}{3}\right) \cdot b \cdot L} \cdot 0.4 \tag{9}$$

where P_a is the dynamic pressure in pounds per square inch measured by the crosstie to ballast transmitter; P is the wheel load in pounds (2P accounting for total crosstie load); L is the crosstie length in inches; b is the crosstie width in inches. The 0.4 factor represents

that 40% of the pressures are distributed on the crosstie directly under the wheel load (Hay 1982).

The P value, according to Talbot (1940), relies on the dynamic load factor, which is a primarily function of the speed of the train. Therefore, as the speed, the pressure at the CT-B interface will proportionally increase. The AREMA 2018 design manual recommends a maximum contact pressure of 448 kPa for wood crossties and a maximum of 586 kPa for concrete crossties.

Russell et al. (2018) measured the real-time dynamic pressures at the CT-B interface at various wheel loadings and train speeds, with each wheel loading variation producing different trackbed pressure measurements. The averaged trackbed pressures produced by the variable speeds of the FRA test cars are shown in Figure 3.5.

Note that as the speed increases to the maximum speed permitted on this line, the CT-B pressure decreases slightly for a given wheel loads.

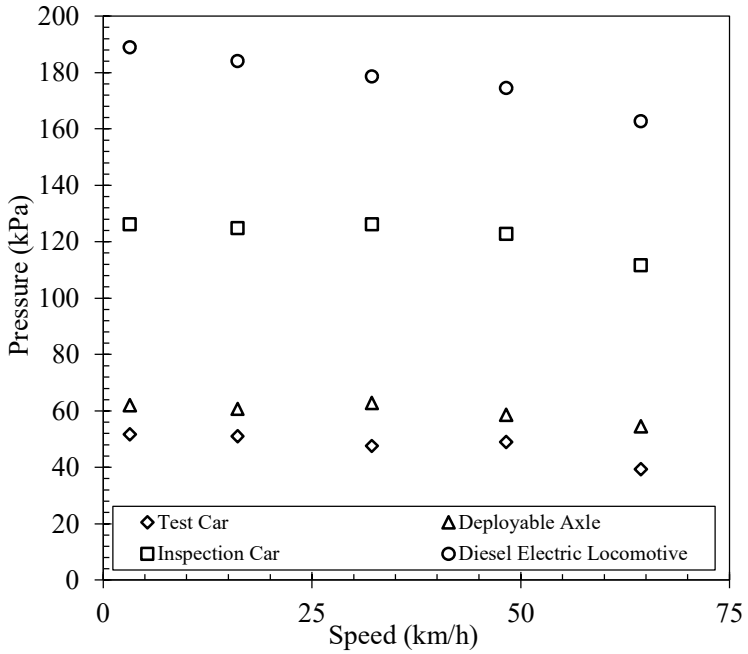

Figure 3.5 Plot of trackbed pressures of the FRA test train experiment at various train travel speeds.

The SD60E locomotive produced the highest test dynamic pressures among the FRA test cars ranging from 165 kPa to 186 kPa. The inspection car (DOTX 220) produced pressures ranging from 110 kPa to 124 kPa, with the deployable axle producing approximately 55 kPa to 62 kPa of pressure and the remaining axles producing 41 kPa to 55 kPa of pressure per axle.

The findings of this research show that the dynamic contact pressures are highly dependent on the magnitudes of wheel loadings and minimally dependent on speed. Therefore, this paper challenges the traditional Talbot (1940) methodology. The highest pressure experienced is 207 kPa, nearly half of the Talbot (1940) recommended design values for wood crossties. Therefore, it can be concluded that the CT-B interface pressures are overestimated by the Talbot (1940) methodology, and speed variation has a minimal effect on the CT-B interfacial pressures.

3.5 THE PRESSURE COMPARISON OF DIFFERENT METHODOLOGIES

In the railroad industry, there are several ways to determine the CT-B interface dynamic contact pressures. Traditionally, the Talbot (1940) and Ahlf (2003) methodologies are the most common. This section compares the Talbot (1940), Ahlf (2003), and square wave methodologies (Unluoglu et al. 2022) to the experimentally measured data. Equation 1 and Equation 9 are used to determine the Ahlf (2003) and Talbot (1940) methodology pressures, respectively, while the square wave methodology (Unluoglu et al. 2022) uses Equation 5. Table 3.3 shows assumptions made during calculations involving these equations, and Figure 3.6 compares the three methodologies.

Table 3.3 Calculation assumptions for Talbot (1940) and Ahlf (2003) methodologies.

Variable	Definition	Magnitude
D	Wheel diameter	838.2 mm
b	Crosstie width	228.6 mm
L	Crosstie length	2,590.8 mm
T	Multiplier value	1
S	Center to center spacing	508 mm
U	Track modulus	20.7 MPa
E	Modulus of rail	210,000 Mpa
I	Moment of inertia of rail	94.2 in^4

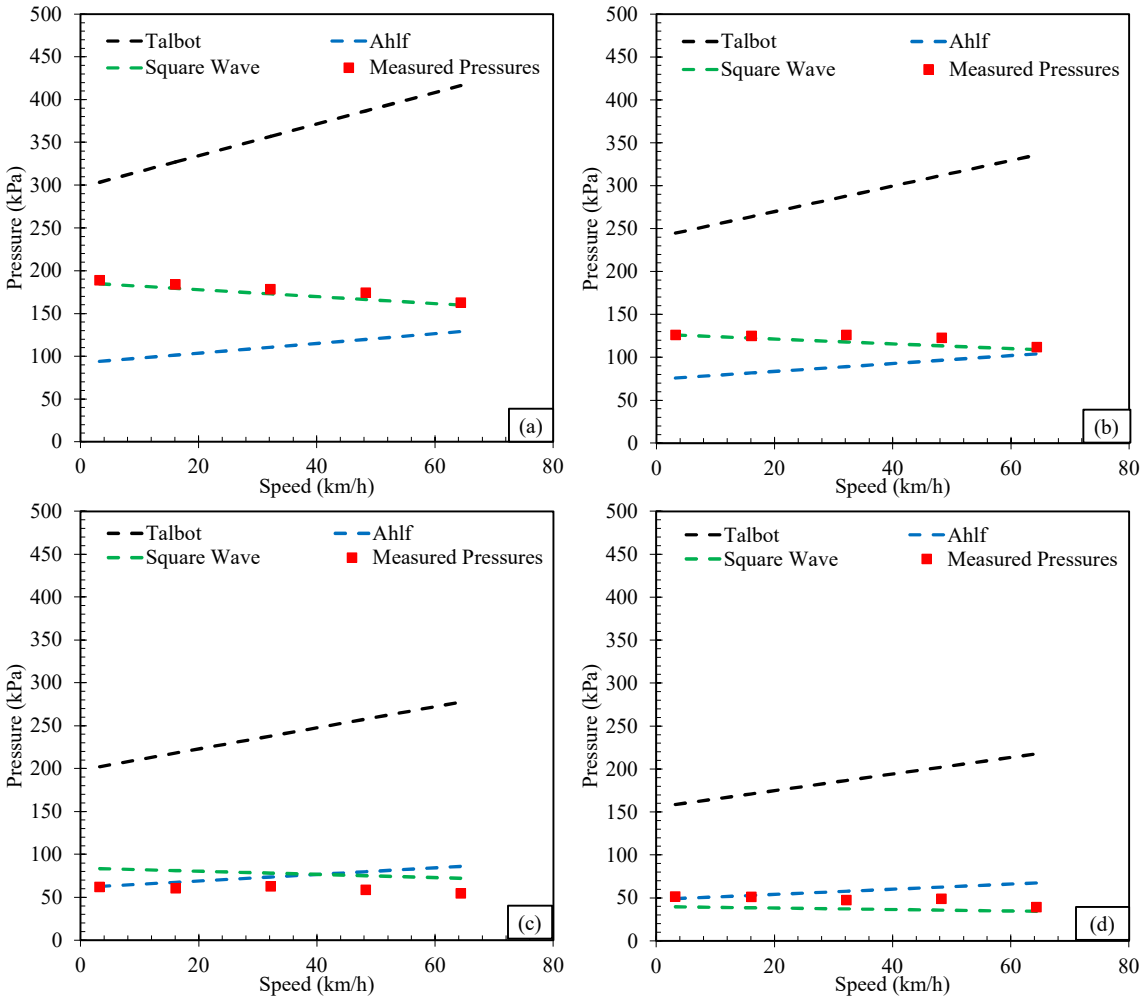

Figure 3.6 The comparison of Talbot (1940), Ahlf (2003), and square wave methods to calculate pressure for various operation speeds with wheel loads as follows: (a) 147 kN; (b) 118 kN; (c) 98 kN; (d) 77 kN.

Figure 3.6 shows the results for the Talbot (1940) method significantly overestimated pressures as compared to the Ahlf (2003) and square wave methods. The Talbot (1940) method determines that the contact pressure is 444 kPa at a travel speed of 64 km/h, while the experimentally measured pressure is 163 kPa at the same travel speed. The difference between the Talbot (1940) method and the other measures become more distinguishable at greater speeds as the Talbot (1940) method obtains a dynamic load using the speed-dependent dynamic load factor. On the other hand, the Ahlf (2003) method is accurate to the experimentally measured data for lower wheel loadings. As wheel load

increases, the accuracy of the Ahlf (2003) method to the experimentally measured data decreases. The square wave method (Unluoglu et al. 2022) predicted dynamic contact pressures at the CT-B interface are the most similar in magnitude to the experimentally measured pressure data. Additionally, the trend of the data for the Ahlf (2003) and Talbot (1940) pressures increased with increasing travel speed, whereas the experimentally measured data and predicted pressures tend to decrease.

In conclusion, the difference between the traditional Talbot (1940) method and the experimentally measured pressures are significant. The Talbot (1940) method predicts upwards of three times the experimentally measured pressures. Since the difference between these methods is considerable, the traditional Talbot (1940) method to predict trackbed dynamic pressures at the CT-B interface may be an extremely overestimating method.

Ahlf (2003) stated that the current AREMA maximum stress recommendation at the bottom of ballast (170 kPa) is grossly in excess. The Ahlf (2003) analysis supports the findings of this paper as Ahlf notes that the pressures at the bottom of the ballast are a function of the pressure at the CT-B interface. These findings indicate that the AREMA (2018) recommendation value of 448 kPa should be reevaluated and possibly replaced with a lower, more accurate value of CT-B interface pressure for the design.

3.6 THE LONGITUDINAL PRESSURE DISTRIBUTION OVER THE ADJACENT CROSSTIES

Understanding stress distribution throughout the railroad track is critical for high-performance track design. Quality track design requires less maintenance and offers increased efficiency and value. To understand this stress distribution, it is important to

determine the stresses on the top of the ballast (also called the CT-B interfacial pressures in this paper). Pressure distribution both vertically (experienced beneath the rail/wheel) and longitudinally is vital to understanding stress distribution throughout the railroad track.

Early design methodologies, such as Talbot (1940), assumed that the wheel loads are distributed over three crossties; 40% of the wheel loads are distributed to the crosstie directly below the wheel, and the rest are distributed over the adjacent crossties, which vary with crosstie spacing (Hay 1982). This paper analyzes test data conducted by Russell et al. (2020) to confirm that these assumptions are accurate for heavier wheel loads.

Multiple tests were conducted with various wheel loads of 44 kN, 67 kN, 89 kN, and 98 kN to quantify the longitudinal static distribution of the CT-B interfacial pressures in Mascot, TN in 2018. The deployable axle of the FRA test train (DOTX 218) was utilized during testing. Pressure measurements were collected simultaneously by pressure cells placed at the CT-B interface directly beneath the crossties under the deployable axle and adjacent crossties. This static stress distribution data is shown in Figure 3.7.

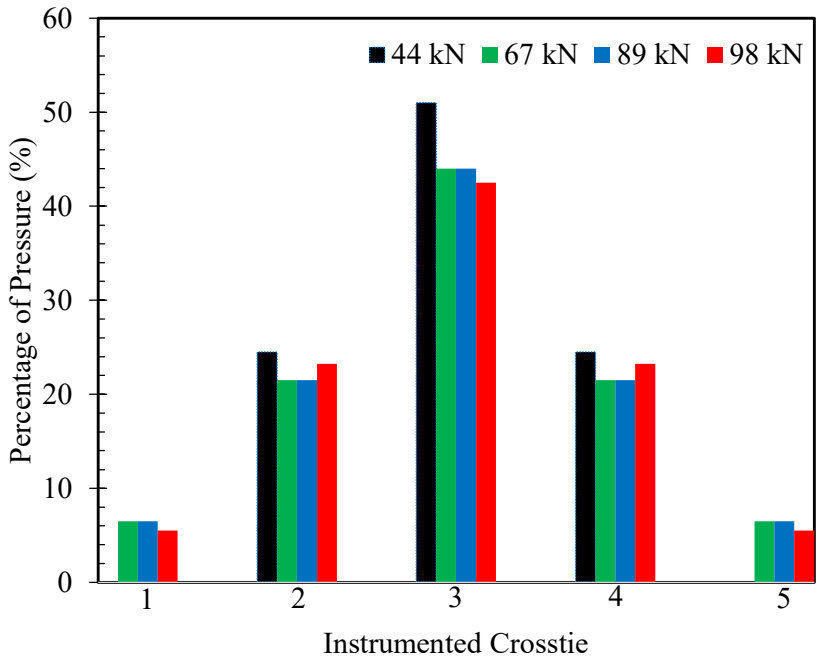

Figure 3.7 Static longitudinal pressure distribution over crossties due to various wheel loads.

Loading pressures are distributed over five crossties, as shown in Figure 3.7. Two crossties are located on either side of the deployable axle (a total of four crossties, two on each side), and one central crosstie is located (loaded) directly beneath the axle. Crosstie 3 (center) is the crosstie directly under the deployable axle, where Crosstie 2 and Crosstie 4 are the adjacent crossties, as shown in Figure 3.7. Note that the recorded pressures for the 44 kN static load, the lowest applied load, were distributed over only the three central crossties. It was determined that, with the exception of the 44 kN load, the pressures could extend up to 1524 mm longitudinally from the load in each direction (using 508 mm center-to-center crosstie spacing). Averages of the data indicate that the central crosstie directly under the deployable axle experienced roughly 45% of the total pressure. In comparison, the two directly adjacent crossties each experienced approximately 22.5% of the total pressure, and the two outermost crossties each experienced approximately 5% of the total

pressure. Since the data is comparable to a normal distribution, a symmetrical bell-shaped curve, a Gaussian Distribution equation was developed to predict the pressures experienced over the adjacent crossties based on the wheel loadings.

Unluoglu et al. (2022) developed an equation to predict static pressures at the CT-B interface based on the measured data. This equation (Unluoglu et al. 2022) predicts the pressures directly under the wheel loadings and is expressed as 21.93% of the total load/pressure. The longitudinal and lateral pressure distribution should be considered together to extend the knowledge of entire crosstie-ballast interfacial pressures. The crosstie directly under the wheel is exposed to 43% of the entire load/pressure. In light of this information, the function of the bell-shaped curve based on the wheel loading can be expressed as:

$$f(x) = \left[0.08679 \cdot \left(P_s \cdot \alpha\right)^{2.219}\right] \cdot \beta \cdot \exp\left[-\left(\frac{x-C}{1.325}\right)^2\right] \tag{10}$$

where x is the crosstie number; C is the center crosstie; P_s is the static wheel loading; α is the distribution factor of 21.93%; β represents the ratio of 43% to 21.93%; 1.325 is related to the curve width. Since the static pressure is distributed over five crossties, x must be an integer and varies between 1 and 5 and C value is 3. The equation can be simplified as:

$$f(x) = \sigma_s \cdot \beta \cdot \exp\left[-\left(\frac{x-C}{1.325}\right)^2\right] \tag{11}$$

where σ_s is the static pressure due to the static wheel load. Figure 3.8 shows representing the bell-shaped curve for various wheel loadings.

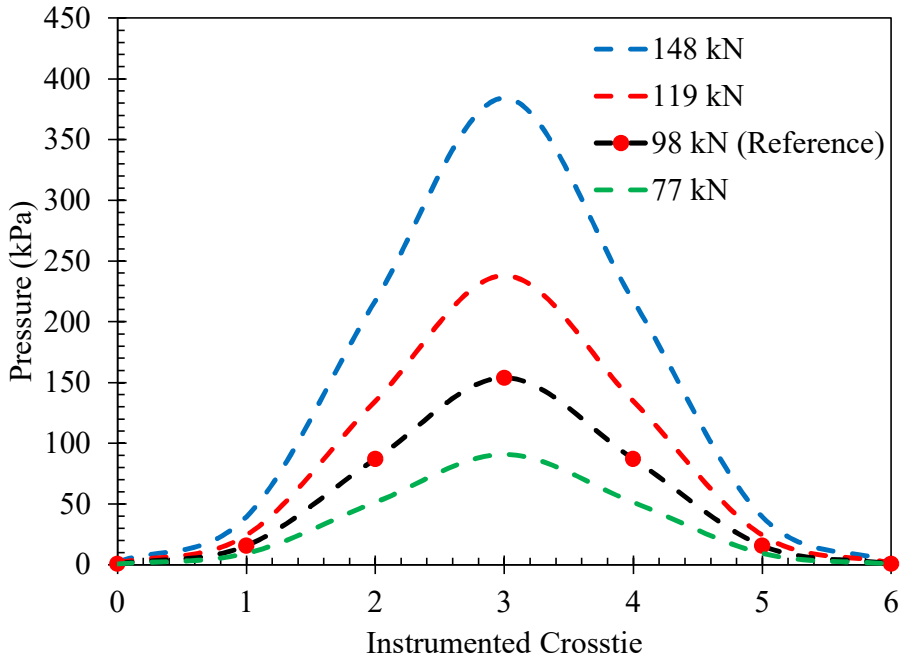

Figure 3.8 Predicted Pressure Distribution over the crossties at various wheel loads based on the Gaussian Distribution equation.

This paper represents the measured stress distributions as a percentage and confirms the known recommended practice (AREMA 2018) to a certain degree. The recommended practice (AREMA 2018) reports that the pressures are distributed over three crossties. The crosstie directly under the wheel and the next two are exposed to 40% and 30%, respectively. According to the measured data, the crosstie directly under the wheel, the adjacent two and the outer two crossties are exposed to 45%, 22.5% and 5%, respectively. However, it is important to realize that crosstie spacing influences the pressure distribution percentages over the crossties.

Having a better understanding of pressure distribution over adjacent crossties may contribute to maintenance. For instance, ballast degradation occurs due to the loads above the ballast. If the stresses over the ballast are known, a favorable schedule may be implemented for replacing or maintaining the ballast. Even the ballast degradation might

be controlled to a certain degree. By practicing the pressure distribution over the crossties, the life cycle of the crossties and ballast may be determined more accurately.

3.7 THE LOAD/PRESSURE DISTRIBUTION ALONG THE CROSSTIE

The objective of this section is to analyze measured CT-B interfacial pressures along the crosstie. A half-size experimental trackbed was assembled in the laboratory with four recessed earth pressure cells (EPCs) as shown in Figure 3.9. The crosstie consisted of a half-length crosstie with an additional length for the pressure cell positioned at the center of the complete crosstie. The applied static loads varied from 6.7 kN to 47 kN. Multiple tests were conducted for each combination of loading intensities. Pressure intensities were selected to provide measured CT-B pressures under the rail in excess of the range measured in the in-track tests.

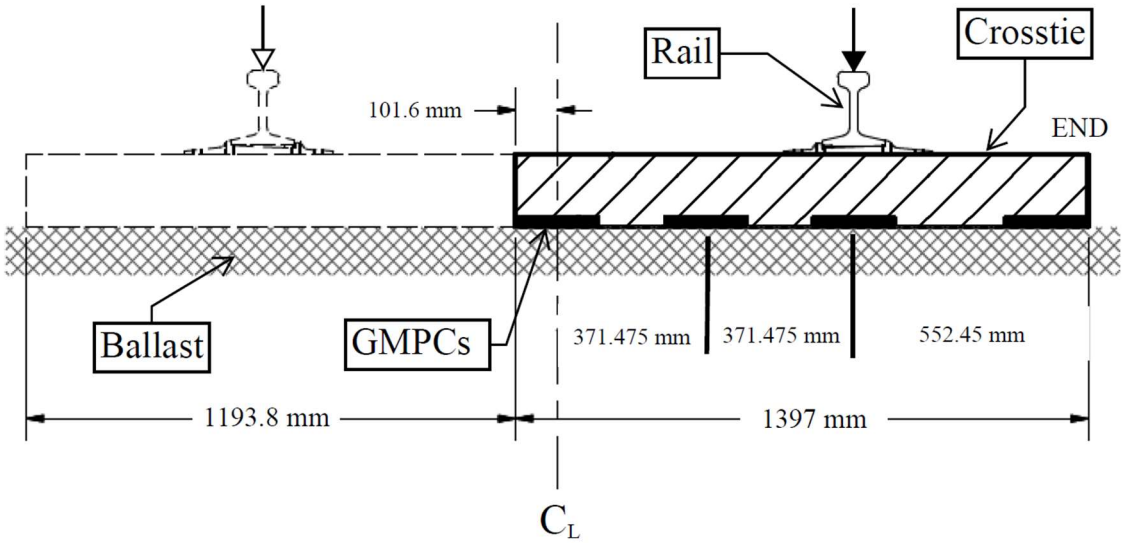

Figure 3.9 Schematic of half-length crosstie with four embedded EPCs with resilient support and simulated rail loading used in laboratory testing (after Russell et al. 2020).

The typical stress distribution intensities along the crosstie and the normalized percentage pressure distribution based on the ratio of the distance from the crosstie center to wheel diameter are shown in Figure 3.10.

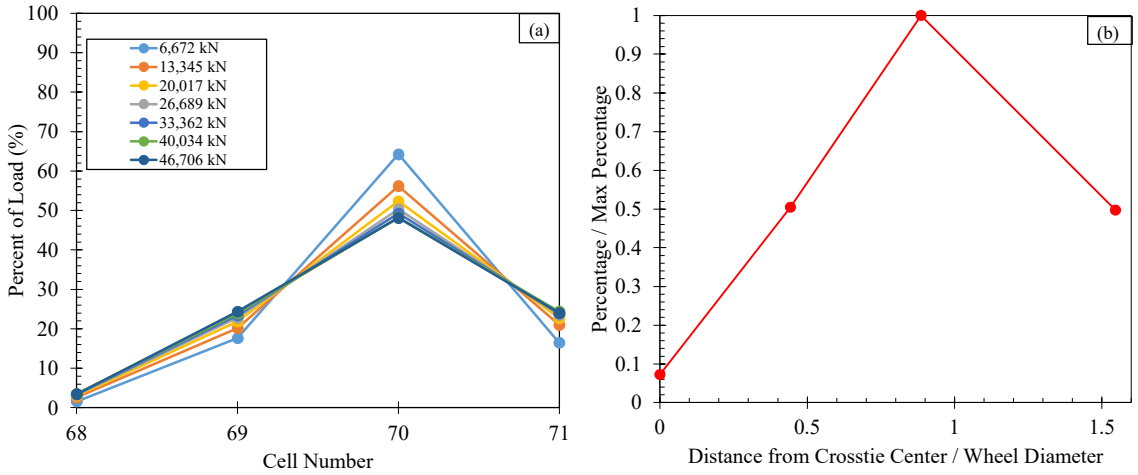

Figure 3.10 (a) Percentage of load/pressure carried by a half-length crosstie from laboratory testing; (b) The normalized percentage pressure distribution based on the ratio of the distance from the crosstie center to the wheel diameter.

The maximum pressure occurs directly under the rail. This pressure intensity accounts for approximately half of the total transferred load (Russell et al. 2020). Less than 3% of the total load exists at the center portion of the crosstie. The outer section of the crosstie and the point mid-way between the rail and center portion of the crosstie experience 20 to 25% of the total transferred load.

The typical stress distribution intensities along the crosstie were normalized based on the ratio of the distance from the crosstie center to the wheel diameter. The wheel diameter was assumed to be 838 mm. Table 3.4 shows the normalized values:

Table 3.4 The normalized magnitudes.

y	x
0.072	0
0.504	0.443
1	0.886
0.497	1.546

where x is the ratio of the distance from the crosstie center to 838 mm of a wheel diameter; y is the ratio of the percent of the pressure distributions at that location to the maximum percentage of the pressure distribution (directly under the wheel).

3.8 COMPARISON OF THE LOAD/PRESSURE DISTRIBUTION ON THE CROSSTIE TO THE TRADITIONAL METHOD

This section discusses the stress distribution at the CT-B interface of a single wheel on an all-granular trackbed. In addition to this, the distribution will be compared to the traditional Talbot (1940) methodology. The stress distribution along the crosstie was discussed previously. Since 47 kN was the highest and most similar loading in real traffic conditions, the 47 kN curve was used as a reference. The percent of load distribution corresponding to the highest value was reported as 3% for Cell 68, 22% for Cell 69, 51% for Cell 70, and 24% for Cell 71. If the longitudinal pressure distribution and the pressure distribution along the crosstie are analyzed together, a distribution map can be developed longitudinally and laterally. Table 3.5 shows the load distribution over and along the crosstie. This table has considered that the wheel loads are far enough not to overlap their pressures with each other.

Table 3.5 The load distribution along a crosstie.

Cell	Instrumented Crosstie				
	1	2	3	4	5
Cell 68	0.16%	0.79%	1.58%	0.16%	0.79%
Cell 69	1.13%	5.53%	11.06%	1.13%	5.53%
Cell 70	2.23%	10.92%	21.93%	2.23%	10.92%
Cell 71	1.11%	5.45%	10.90%	1.11%	5.45%

Recommended practice (AREMA 2018) states that the stress distribution along the crosstie occurs on the outer two-thirds of the crosstie, and the center section does not experience any loads. In theory, the load distribution is more likely a rectangular shape (uniform). However, the findings of this research disagree with this recommended practice. The load is distributed along the crosstie with maximum occurring under the rail as shown in Table 3.5. The CT-B interface directly under the wheel loading has the highest percentage (21.93%), and the pressures decrease through the center point of the crosstie. The measured pressures resemble a bell curve, unlike the state of recommended practice uniform distribution. Figure 3.11 illustrates the distribution of real-time loads on the half-crosstie. Load and pressure distribution is assumed to be symmetrical on the other side of the crosstie.

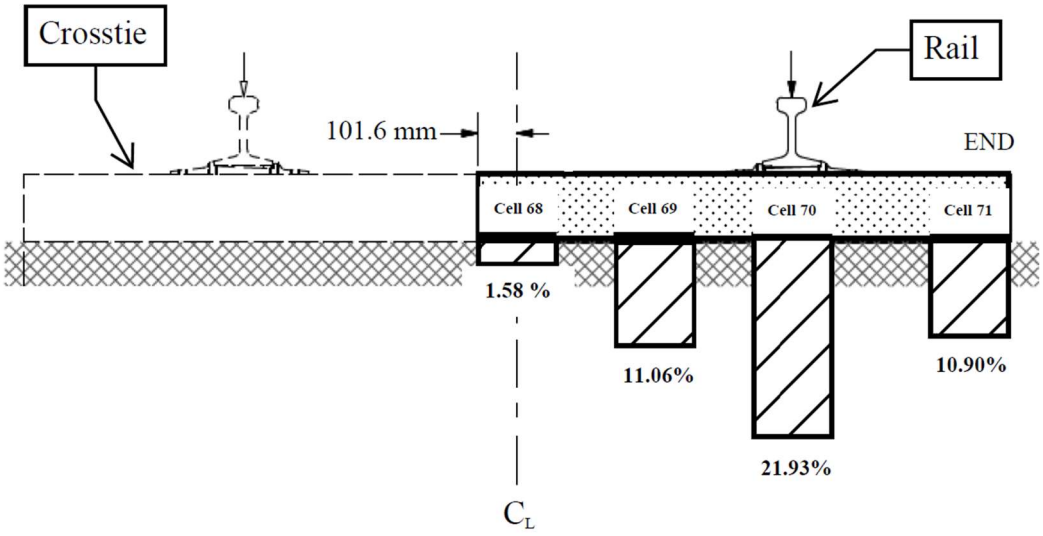

Figure 3.11 The pressure distribution of measured pressure.

Figure 3.11 shows that the assumption the total load/pressure is distributed over two-thirds of the crosstie is unconservative. Therefore, this paper recommends that the two-third coefficient of Equation 9 be changed. In addition, the crosstie is commonly analyzed as a square footing in the railroad track design. However, loads are not distributed equally along the crosstie. In total, less than half of the loads are distributed directly under the wheel load. Therefore, the longitudinal and lateral load distribution should be analyzed as combined.

3.9 BALLAST STRESS DISTRIBUTION

The ballast is a vital track element to transmit and distribute axle loads from the crossties to the underlying subballast and subgrade at a minimized level (Selig and Waters 1994). Due to the cycled loads, ballast becomes degraded and fouled. This degradation and fouling process occurs by the progressive accumulation of fines within the ballast voids (Indraratna et al. 2011). More than 373,000 kilometers of railroad track must be

periodically evaluated and continually maintained in the US. An accurate track assessment is a must to minimize maintenance costs to adequately maintain the track system (Al-Qadi et al. 2010). A better understanding of the pressure distribution through the ballast may contribute positively to track design and accurate track assessment.

The traditional methods, such as the Talbot method (1940), led the railroad industry for many years. Talbot (1940) developed an empirical formula to calculate the pressure at the bottom of the ballast (Hay 1982). The equation is a function of unit pressure over the outer two-thirds bearing area of the crosstie, the depth below that bearing surface, and the crosstie pressure (American Railway Engineering Association, 1980).

According to the recommended design manual (AREMA 2018), the value is around 448 kPa for timber crossties, which is overestimated compared to the measured data. Since the obtained pressures are minimal compared to the Talbot (1940) equation values, the ballast pressures may be less than the recommended 138 kPa. More specifically, 138 kPa is questionable as a recommended value. On the other hand, the minimum ballast thickness can be rearranged to attain 138 kPa. According to Hay's (1982) textbook, a minimum desirable depth of ballast of 622 mm is indicated. However, almost no private railroad company uses this desired depth of ballast. Instead, railroad companies commonly use 304.8 mm in their railroad designs. Therefore, the pressures at the bottom of the ballast will be even greater than the recommended ballast pressure value.

The Talbot (1940) equation to determine ballast pressures analyzes the crosstie as a square footing. However, the load/stress distribution along the crosstie is ununiform. This is because the pressure distribution influence lines through the ballast may be unrepresentative. This paper recommends either future research or the development of

Finite Element models based on pressure distribution along the crosstie is desirable to determine new influence lines.

3.10 CONCLUSIONS AND RECOMMENDATIONS

This section covers the conclusions and recommendations based on the comparisons between traditional methods (e.g., Talbot 1940 and Ahlf 2011), the square wave theory (Unluoglu et al. 2022), and the in-track data obtained from the FRA test train in Mascot, TN, in 2018.

Firstly, quantifying stress distributions at the interface of the CT-B would be considerably helpful for track design and analysis. GMPCs (also called earth pressures) are an advanced and recommended way to measure the pressure in railroad track. For this research, smooth wheels were confirmed in a WILD installation at Ebenezer, TN, before conducting tests since wheel or track irregularities may cause high-impact pressure indications on pressure cells.

Moreover, this paper does not support the thesis that the pressure at the CT-B interface increases by speed. Instead, the measured data indicates that speed has a minimum effect on the CT-B interfacial pressures. Specifically, pressures decrease slightly as the speed increases.

This paper compares and analyzes the Talbot (1940), the Ahlf (2003), and the square wave methodology (Unluoglu et al. 2022) pressure magnitudes with the in-track measured pressures. It is noted that pressures based on the Talbot (1940) methodology are nearly three times higher than the Ahlf (2003) methodology, measured data, and the square wave (Unluoglu et al. 2022) pressures. The pressures at the CT-B interface are overestimated as

using the Talbot (1940) methodology. Additionally, the Ahlf (2003) calculations also indicate that the pressures at the bottom of the ballast are overestimated. Since subgrade pressures (at the bottom of ballast) are a function of CT-B interfacial pressures, Ahlf (2003) supports this paper's proposition. This research recommends that AREMA reduce the typical maximum permitted pressure values to more reasonable ones.

Subsequently, this paper confirms the state of practice for the longitudinal stress distribution over the crosstie. The recommended design manual (AREMA 2018) states the pressures are distributed over three crossties. The crosstie directly below the wheel experience 40% of the wheel load, and each adjacent crosstie experiences 30%. This paper states that the pressures are distributed over five crossties in static conditions. The crosstie under the wheel supports nearly 45% of the load, while the two adjacent crossties are each exposed to around 22.5%. The next two crossties are each exposed to 5%. However, crosstie spacing may slightly change these distribution percentages.

Unlike the longitudinal stress distribution, there is little information about the stress distribution along the crossties in the literature. Traditional methods (Talbot 1940) assume that the load distribution along the crosstie is uniform, with the outer two-thirds of the crosstie distributing the loads and the center of the crosstie experiencing no pressure. However, this research shows that the load distribution along the crosstie is not uniform. The area midway directly under the rail experiences nearly 22% of the loads. The end portion of the crosstie experiences slightly less than 11% while the center of crosstie experiences 1.5%. The area between the center of the crosstie and the area directly under the rail experiences slightly over 11% of the load.

This research indicates that the crosstie cannot be analyzed as a square footing because the loading along the crosstie is not uniform. Lastly, this research recommends that the longitudinal and lateral stress distributions be considered when evaluating trackbed pressure distributions.

3.11 ACKNOWLEDGEMENTS

This research was primarily funded by the National University Rail Center (NURail). A special thanks to prior Graduate Assistants Ethan Russell and Travis J. Watts, Visiting Scholar Qinglie Liu, and Dr. David Clark for their significant contributions during the early phases of this research. The cooperation and contributions of Norfolk Southern Corporation during the test site installation activities and continued monitoring activities are greatly appreciated. I also acknowledge the contribution to this research by the Federal Railroad Administration Office of Research Development and Technology, ENSCO Inc., and the Volpe National Transportation Systems Center. A special thanks to the Turkish government and the Ministry of Education for their financial support.

4 SUMMARY AND CONCLUSIONS

The uncertainty of stress distribution through the railroad track has been always an issue for the railroad industry. Since the ballast is one of the fundamental components of the railroad track, a significant amount of maintenance expenses occurs in the ballast, estimated at a half billion dollars annually for 150,000 km of Class I track. Therefore, having a better idea of stress distribution may contribute to the track design, which will lead to fewer maintenance requirements in the future.

The recommended practice (AREMA 2018) to determine the pressure in railroad track is based on the works of Talbot (1940). Even though Talbot's (1940) work is a pioneer in railroad history, it is outdated for the modern railroad industry. It is no longer valid for several reasons: the pressure measurement method, inconsistency of supporting conditions, new track design methods (asphalt layer), improved rail (e.g., continuous welded rail), crosstie material properties, significantly increased wheel loadings and traffic, and so on. Therefore, the Talbot (1940) empirical equations are questionable in determining dynamic pressures through the railroad track.

This paper represents an advanced method to measure the CT-B interfacial dynamic pressures. The pressures were measured in Mascot, TN, by using FRA test trains. The pressure cells were placed at the CT-B interface for a time interval to have the closest pressures to the real traffic conditions. To prevent undesired impact loadings (which are more likely a result of wheel irregularities), the test trains traversed a nearby WILD installation at Ebenezer, TN. The WILD data confirmed that the wheels were smooth enough to minimize impact loadings.

A new method was developed based on the obtained data to predict static and dynamic contact pressures at the CT-B interface. This method uses a square wave theory. The amplitude of the square wave represents the average pressures, while the width stands for the length of the bogie. Several equations were proposed to calculate the static/dynamic pressures and affected wheel distances. An algorithm was written to predict pressure for an unlimited number of trains when the basic information of the trains, such as the weight of the train, wheel spacing, speed, number of axles, and coupler lengths, are given.

Additionally, this paper disagrees with the statement that the pressures at the CT-B interface increase by speed. The train speed hardly contributes to the pressures; in other words, the pressures slightly decrease while the speed increases.

This paper analyzed and compared the obtained data with the traditional methods such as the Talbot (1940), the Ahlf (2003), and the square wave theory methodologies. In summary, it is shown that the Talbot (1940) pressures are approximately 300% greater than the Ahlf (2003), square wave, and measure pressures. Therefore, based on this information, this paper deduces that the pressures at the CT-B interface have been overestimated since the Talbot (1940) methodology. This deduction is supported by the Ahlf (2003) analysis that the pressures at the bottom of the ballast are overestimated. Since subgrade pressures are functions of CT-B interfacial pressures, the analysis of Ahlf (2003) supports this paper's proposition. This paper recommends that AREMA reduce the recommended pressure values to more proper values.

Moreover, this paper confirms the recommended practice (AREMA 2018) for the longitudinal stress distribution over the crosstie to a certain degree. The recommended practice (2018) expresses that pressures are distributed over three crossties. The crosstie

directly below the wheel is exposed to 40% of the wheel load, while adjacent crossties experience 30% of the wheel load. This paper reports that the pressures are distributed over five crossties for static conditions. The center crosstie is exposed to nearly 45% of the load, the adjacent crossties experiences around 22.5% of the load, and the outer two crossties are exposed to 5% each. However, the center-to-center crosstie spacing should be considered since the longitudinal stress distribution is a function of the distance between crossties.

The literature has little information about the stress distribution along the crossties, unlike the longitudinal stress distribution. The traditional method (Talbot 1940) assumes that the load distribution along the crosstie is uniform, with the outer two-thirds of the crosstie distributing the loads and the center of the crosstie experiencing no pressure. However, this research reports that the load distribution along the crosstie varies. The area directly above the rail (Cell 70) is exposed to around 22% of the load, with the highest pressure as expected. The outer area of the crosstie (Cell 71) is exposed to slightly less than 11%. The center of the crosstie experiences 1.5% of the load (Cell 68), while the area (Cell 69) between the center of the crosstie and the area directly under the rail experiences slightly over 11%. Cell 69 is closer to Cell 70 than Cell 71; it is expected that Cell 69 is exposed to a greater load percentage than Cell 71.

In terms of ballast stress distribution, this paper disagrees with the method that the crosstie is analyzed as a square footing. Since the loads along the crosstie vary, the crosstie load/stress distribution is ununiform and cannot be analyzed as a square footing. This is because the pressure distribution influence lines through the ballast may be unrepresentative.

This paper ultimately recommends future research, the development of FEM models based on pressure distribution along the crosstie (which is desirable in determining new influence lines), and that the longitudinal and lateral stress distributions be considered to design better performing railroad tracks.

APPENDICES

APPENDIX A – GEOKON GRANULAR MATERIAL PRESSURE CELLS (GMPCs)

Information below in the following table can be found in the Instruction Manual Model 3500 Series Earth Pressure Cells listed in the reference section of this document.

Transducer Type	Semiconductor
Material	Stainless Steel
Cell Dimensions (H x D)	6 x 230 mm (0.25 x 9 in)
Transducer Dimensions (L x D)	150 x 32 mm (6 x 1.25 in)
Pressure Range	Vacuum to 400 bar (6,000 psi)
Fatigue Life	Designed for more than 100 million F.S. cycles
Output	Milllivolt: 100 mV (10 mV/V Voltage:0-5 VDC Current: 4-20 mA (2 wire)
Standard Ranges	100, 250, 400, 600 kPa; 1, 2.5, 6 MPa; 145, 362, 870 psi
Over Range	1.5 x rated pressure
Accuracy	± 0.25 % F.S.
Thermal Effect on Zero	0.05 % F.S.
Linearity	0.5 % F.S.
Temperature Range	-20 °C to +80 °C (-4 °F to 176 °F)
Resolution	Infinite
Excitation Voltage	Millivolt: 10 VDC regulated Voltage: 6.5 – 35 VDC

	Current: 24 VDC (7-35 VDC)
Excitation Frequency	N/A

Typical Pressure Transducer Calibration Report has been shown in the following figure.

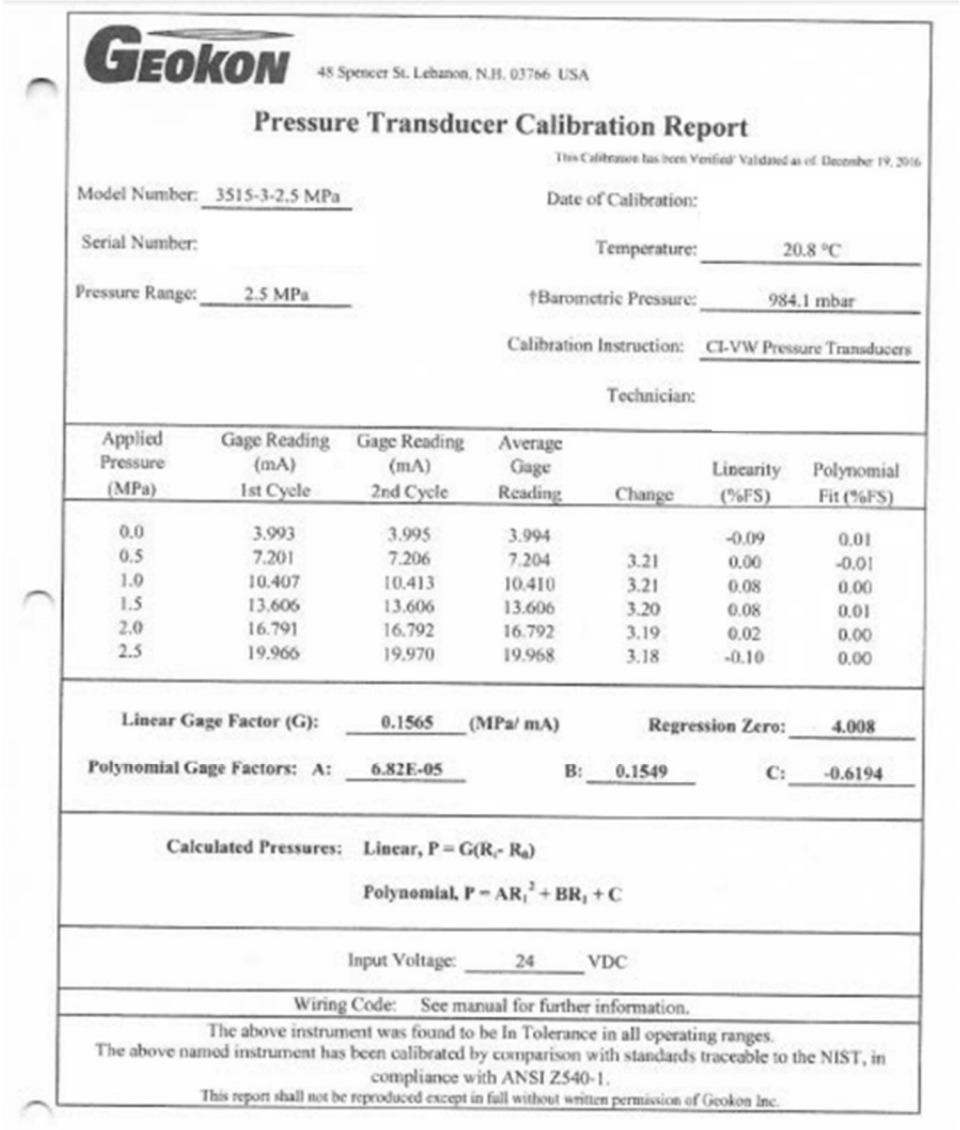

GEOKON 45 Spencer St. Lebanon, N.H. 03766 USA

Pressure Transducer Calibration Report

This Calibration has been Verified/ Validated as of: December 19, 2016

Model Number: 3515-3-2.5 MPa
Date of Calibration:

Serial Number:
Temperature: 20.8 °C

Pressure Range: 2.5 MPa
†Barometric Pressure: 984.1 mbar

Calibration Instruction: CI-VW Pressure Transducers

Technician:

Applied Pressure (MPa)	Gage Reading (mA) 1st Cycle	Gage Reading (mA) 2nd Cycle	Average Gage Reading	Change	Linearity (%FS)	Polynomial Fit (%FS)
0.0	3.993	3.995	3.994		-0.09	0.01
0.5	7.201	7.206	7.204	3.21	0.00	-0.01
1.0	10.407	10.413	10.410	3.21	0.08	0.00
1.5	13.606	13.606	13.606	3.20	0.08	0.01
2.0	16.791	16.792	16.792	3.19	0.02	0.00
2.5	19.966	19.970	19.968	3.18	-0.10	0.00

Linear Gage Factor (G): 0.1565 **(MPa/ mA)** **Regression Zero:** 4.008

Polynomial Gage Factors: A: 6.82E-05 **B:** 0.1549 **C:** -0.6194

Calculated Pressures: **Linear, $P = G(R_i - R_0)$**

Polynomial, $P = AR_i^2 + BR_i + C$

Input Voltage: 24 VDC

Wiring Code: See manual for further information.

The above instrument was found to be In Tolerance in all operating ranges.
The above named instrument has been calibrated by comparison with standards traceable to the NIST, in compliance with ANSI Z540-1.

APPENDIX B – AHLF EXAMPLE CALCULATION STEPS WITH ASSUMPTIONS AND INPUT PARAMETERS

Calculations steps have been provided at 76.7 kN (17.25 kips) of wheel load. The calculations have been done in Mathcad 7.0 Prime (PTC 2021).

INPUT VARIABLES:

$V := 0\ mph$	Velocity (static conditions)
$D_w := 40\ in$	Wheel Diameter
$S := 20\ in$	Center to center tie spacing
$E := 30000000\ \frac{lbf}{in^2}$	Modulus of Rail
$I := 94.2\ in^4$	Moment of Inertia of Rail
$C := 3.35\ in$	Distance between rail neutral axis and location at which F is to be computed, usually at the rail base to maximize C.
$S_h := (23.7)\ in^3$	Section modulus of head (AREMA Figure 4-1-5).
$S_b := (28.2)\ in^3$	Section modulus of base (AREMA Figure 4-1-5).
$B := 11\ in$	Width of Tie
$L := 102\ in$	Length of Tie
$TP_W := 6\ in$	Width of Tie Plate
$TP_L := 11\ in$	Length of Tie Plate
$U := 4000\ \frac{lbf}{in^2}$	Track Modulus
$P_c := 2000\ psf$	Allowable Bearing Pressure of the Subgrade

CALCULATION:

$P_S := 17.250\ kip$ — Single (Static) Wheel Load of Design Car

$\theta := \frac{0.0052 \cdot V}{D_w}$ $\theta := 0$ — Theta will be zero since we are looking at static conditions.

$P_V := P_S + \theta \cdot P_S = 17.25\ kip$ — Single (Dynamic) Wheel Load of Design Locomotive, which is equal to static wheel load since we are looking at static conditions.

$\alpha := 1$ — Since the velocity is less 40 km/hr.

$P_{V1} := \frac{P_V}{1\ kip} \cdot 1000 = 1.725 \cdot 10^4$

$W_0 := \left(315 - \frac{21200}{\left(\frac{P_{V1}}{1120}\right) \cdot \alpha + 67}\right) \cdot 1\ \frac{lb}{yd} = 57.724\ \frac{lb}{yd}$ — Minimum Rail Weight per EQ 6-5 (Ref. TI 850-02)

$X_1 := \frac{\pi}{4} \cdot \left(\frac{4 \cdot E \cdot I}{U}\right)^{\frac{1}{4}} = 32.202\ in$

$X_2 := X_1 \cdot 3 = 96.606\ in$

$D_{12} := 8\ ft + 2\ in = 98\ in$

$D_{23} := (53\ ft + 10\ in) - 2 \cdot D_{12} = 450\ in$

$D_{34} := D_{12} = 98\ in$

To be persistent, inspection car's wheel dimensions are used for all calculations.

$$a := \frac{D_{12}}{X_2} = 1.014 \qquad d := \frac{D_{12}}{X_1} = 3.043$$

$$\frac{D_{23}}{X_2} = 4.658 \qquad \frac{D_{23}}{X_1} = 13.974$$

$$b := \frac{D_{12} + D_{23}}{X_2} = 5.673 \qquad e := \frac{D_{12} + D_{23}}{X_1} = 17.018$$

$$c := \frac{D_{12} + D_{23} + D_{34}}{X_2} = 6.687 \qquad f := \frac{D_{12} + D_{23} + D_{34}}{X_1} = 20.061$$

$$\begin{bmatrix} 0 \\ a \\ b \\ c \end{bmatrix} = \begin{bmatrix} 0 \\ 1.014 \\ 5.673 \\ 6.687 \end{bmatrix} \qquad \begin{bmatrix} 1 \\ 0.01 \\ 0 \\ 0 \end{bmatrix}$$ From Ahlf Graph

$$T_1 := 1 - 0.01 + 0 + 0 = 0.99$$

$$\begin{bmatrix} 0 \\ d \\ e \\ f \end{bmatrix} = \begin{bmatrix} 0 \\ 3.043 \\ 17.018 \\ 20.061 \end{bmatrix} \qquad \begin{bmatrix} 1 \\ -0.15 \\ 0 \\ 0 \end{bmatrix}$$ From Ahlf Graph

$$B_1 := 1 - 0.14 + 0 + 0 = 0.86$$

$$Y := \frac{T_1 \cdot P_V}{2 \cdot U} \cdot \sqrt[4]{\frac{U}{4 \cdot E \cdot I}} = 0.052\ in$$ Track Deflection Ref #3, Fig. O-V

$$L_R := \frac{T_1 \cdot P_V \cdot S}{2} \cdot \left(\frac{U}{4 \cdot E \cdot I}\right)^{\frac{1}{4}} = 4.165\ kip$$ Rail Seat Load Ref #3, Fig. O-V

$$A_{TP} := TP_W \cdot TP_L = 66\ in^2$$ Area of tie plate

$$R := \frac{T_1 \cdot P_V \cdot S}{2 \cdot A_{TP}} \cdot \left(\frac{U}{4 \cdot E \cdot I} \right)^{\frac{1}{4}} = 63.108 \ \frac{lbf}{in^2}$$ Plate Pressure on tie

$$M := \frac{B_1 \cdot P_V}{4} \cdot \left(\frac{4 \cdot E \cdot I}{U} \right)^{\frac{1}{4}} = 152.062 \ in \cdot kip$$ Rail Bending Moment

$$F := \frac{B_1 \cdot P_V \cdot C}{4 \cdot I} \cdot \left(\frac{4 \cdot E \cdot I}{U} \right)^{\frac{1}{4}} = 5.408 \ ksi$$ Rail Bending Stress

$$P_a := \frac{T_1 \cdot P_V \cdot S}{L \cdot B} \cdot \left(\frac{U}{4 \cdot E \cdot I} \right)^{\frac{1}{4}} = 7.425 \ psi$$

$P_a = 51.19 \ kPa$ Static Pressure between crosstie and ballast.

Calculations steps have been provided at 97.9 kN (22 kips) of wheel load.

INPUT VARIABLES:

$V := 0\ mph$	Velocity (static conditions)
$D_w := 40\ in$	Wheel Diameter
$S := 20\ in$	Center to center tie spacing
$E := 30000000\ \frac{lbf}{in^2}$	Modulus of Rail
$I := 94.2\ in^4$	Moment of Inertia of Rail
$C := 3.35\ in$	Distance between rail neutral axis and location at which F is to be computed, usually at the rail base to maximize C.
$S_h := (23.7)\ in^3$	Section modulus of head (AREMA Figure 4-1-5).
$S_b := (28.2)\ in^3$	Section modulus of base (AREMA Figure 4-1-5).
$B := 11\ in$	Width of Tie
$L := 102\ in$	Length of Tie
$TP_W := 6\ in$	Width of Tie Plate
$TP_L := 11\ in$	Length of Tie Plate
$U := 4000\ \frac{lbf}{in^2}$	Track Modulus
$P_c := 2000\ psf$	Allowable Bearing Pressure of the Subgrade

CALCULATION:

$P_S := 22\ kip$ — Single (Static) Wheel Load of Design Car

$\theta := \frac{0.0052 \cdot V}{D_w}$ $\quad \theta := 0$ — Theta will be zero since we are looking at static conditions.

$P_V := P_S + \theta \cdot P_S = 22\ kip$ — Single (Dynamic) Wheel Load of Design Locomotive, which is equal to static wheel load since we are looking at static conditions.

$\alpha := 1$ — Since the velocity is less 40 km/hr.

$P_{V1} := \frac{P_V}{1\ kip} \cdot 1000 = 2.2 \cdot 10^4$

$W_0 := \left(315 - \frac{21200}{\left(\frac{P_{V1}}{1120}\right) \cdot \alpha + 67}\right) \cdot 1\ \frac{lb}{yd} = 70.317\ \frac{lb}{yd}$ — Minimum Rail Weight per EQ 6-5 (Ref. TI 850-02)

$X_1 := \frac{\pi}{4} \cdot \left(\frac{4 \cdot E \cdot I}{U}\right)^{\frac{1}{4}} = 32.202\ in$

$X_2 := X_1 \cdot 3 = 96.606\ in$

$D_{12} := 8\ ft + 6\ in = 102\ in$

$D_{23} := (59\ ft + 6\ in) - D_{12} = 612\ in$

$D_{34} := D_{12} = 102\ in$

To be persistent, inspection car's wheel dimensions are used for all calculations.

$$a := \frac{D_{12}}{X_2} = 1.056 \qquad d := \frac{D_{12}}{X_1} = 3.168$$

$$\frac{D_{23}}{X_2} = 6.335 \qquad \frac{D_{23}}{X_1} = 19.005$$

$$b := \frac{D_{12} + D_{23}}{X_2} = 7.391 \qquad e := \frac{D_{12} + D_{23}}{X_1} = 22.173$$

$$c := \frac{D_{12} + D_{23} + D_{34}}{X_2} = 8.447 \qquad f := \frac{D_{12} + D_{23} + D_{34}}{X_1} = 25.34$$

$$\begin{bmatrix} 0 \\ a \\ b \\ c \end{bmatrix} = \begin{bmatrix} 0 \\ 1.056 \\ 7.391 \\ 8.447 \end{bmatrix} \qquad \begin{bmatrix} 1 \\ -0.01 \\ 0 \\ 0 \end{bmatrix}$$ From Ahlf Graph

$$T_1 := 1 - 0.01 + 0 + 0 = 0.99$$

$$\begin{bmatrix} 0 \\ d \\ e \\ f \end{bmatrix} = \begin{bmatrix} 0 \\ 3.168 \\ 22.173 \\ 25.34 \end{bmatrix} \qquad \begin{bmatrix} 1 \\ -0.14 \\ 0 \\ 0 \end{bmatrix}$$ From Ahlf Graph

$$B_1 := 1$$

$$Y := \frac{T_1 \cdot P_V}{2 \cdot U} \cdot \sqrt[4]{\frac{U}{4 \cdot E \cdot I}} = 0.066\ in$$ Track Deflection Ref #3, Fig. O-V

$$L_R := \frac{T_1 \cdot P_V \cdot S}{2} \cdot \left(\frac{U}{4 \cdot E \cdot I}\right)^{\frac{1}{4}} = 5.312\ kip$$ Rail Seat Load Ref #3, Fig. O-V

$$A_{TP} := TP_W \cdot TP_L = 66\ in^2$$ Area of tie plate

$$R := \frac{T_1 \cdot P_V \cdot S}{2 \cdot A_{TP}} \cdot \left(\frac{U}{4 \cdot E \cdot I} \right)^{\frac{1}{4}} = 80.486 \ \frac{lbf}{in^2}$$ Plate Pressure on tie

$$M := \frac{B_1 \cdot P_V}{4} \cdot \left(\frac{4 \cdot E \cdot I}{U} \right)^{\frac{1}{4}} = 225.505 \ in \cdot kip$$ Rail Bending Moment

$$F := \frac{B_1 \cdot P_V \cdot C}{4 \cdot I} \cdot \left(\frac{4 \cdot E \cdot I}{U} \right)^{\frac{1}{4}} = 8.02 \ ksi$$ Rail Bending Stress

$$P_a := \frac{T_1 \cdot P_V \cdot S}{L \cdot B} \cdot \left(\frac{U}{4 \cdot E \cdot I} \right)^{\frac{1}{4}} = 9.469 \ psi$$

$P_a = 65.286 \ kPa$ Static Pressure between crosstie and ballast.

Calculation steps have been provided at 118.4 kN (26.625 kips) of wheel load.

INPUT VARIABLES:

$V := 0\ mph$	Velocity (static conditions)
$D_w := 40\ in$	Wheel Diameter
$S := 20\ in$	Center to center tie spacing
$E := 30000000\ \frac{lbf}{in^2}$	Modulus of Rail
$I := 94.2\ in^4$	Moment of Inertia of Rail
$C := 3.35\ in$	Distance between rail neutral axis and location at which F is to be computed, usually at the rail base to maximize C.
$S_h := (23.7)\ in^3$	Section modulus of head (AREMA Figure 4-1-5).
$S_b := (28.2)\ in^3$	Section modulus of base (AREMA Figure 4-1-5).
$B := 11\ in$	Width of Tie
$L := 102\ in$	Length of Tie
$TP_W := 6\ in$	Width of Tie Plate
$TP_L := 11\ in$	Length of Tie Plate
$U := 4000\ \frac{lbf}{in^2}$	Track Modulus
$P_c := 2000\ psf$	Allowable Bearing Pressure of the Subgrade

CALCULATION:

$P_S := 26.625\ kip$ — Single (Static) Wheel Load of Design Car

$\theta := \frac{0.0052 \cdot V}{D_w}$ $\quad \theta := 0$ — Theta will be zero since we are looking at static conditions.

$P_V := P_S + \theta \cdot P_S = 26.625\ kip$ — Single (Dynamic) Wheel Load of Design Locomotive, which is equal to static wheel load since we are looking at static conditions.

$\alpha := 1$ — Since the velocity is less 40 km/hr.

$P_{V1} := \frac{P_V}{1\ kip} \cdot 1000 = 2.663 \cdot 10^4$

$W_0 := \left(315 - \frac{21200}{\left(\frac{P_{V1}}{1120}\right) \cdot \alpha + 67}\right) \cdot 1\ \frac{lb}{yd} = 81.449\ \frac{lb}{yd}$ — Minimum Rail Weight per EQ 6-5 (Ref. TI 850-02)

$X_1 := \frac{\pi}{4} \cdot \left(\frac{4 \cdot E \cdot I}{U}\right)^{\frac{1}{4}} = 32.202\ in$

$X_2 := X_1 \cdot 3 = 96.606\ in$

$D_{12} := 8\ ft + 6\ in = 102\ in$

$D_{23} := (59\ ft + 6\ in) - D_{12} = 612\ in$

$D_{34} := D_{12} = 102\ in$

To be persistent, inspection car's wheel dimensions are used for all calculations.

$$a := \frac{D_{12}}{X_2} = 1.056 \qquad d := \frac{D_{12}}{X_1} = 3.168$$

$$\frac{D_{23}}{X_2} = 6.335 \qquad \frac{D_{23}}{X_1} = 19.005$$

$$b := \frac{D_{12} + D_{23}}{X_2} = 7.391 \qquad e := \frac{D_{12} + D_{23}}{X_1} = 22.173$$

$$c := \frac{D_{12} + D_{23} + D_{34}}{X_2} = 8.447 \qquad f := \frac{D_{12} + D_{23} + D_{34}}{X_1} = 25.34$$

$$\begin{bmatrix} 0 \\ a \\ b \\ c \end{bmatrix} = \begin{bmatrix} 0 \\ 1.056 \\ 7.391 \\ 8.447 \end{bmatrix} \qquad \begin{bmatrix} 1 \\ -0.01 \\ 0 \\ 0 \end{bmatrix}$$ From Ahlf Graph

$$T_1 := 1 - 0.01 + 0 + 0 = 0.99$$

$$\begin{bmatrix} 0 \\ d \\ e \\ f \end{bmatrix} = \begin{bmatrix} 0 \\ 3.168 \\ 22.173 \\ 25.34 \end{bmatrix} \qquad \begin{bmatrix} 1 \\ -0.14 \\ 0 \\ 0 \end{bmatrix}$$ From Ahlf Graph

$$B_1 := 1 - 0.14 + 0 + 0 = 0.86$$

$$Y := \frac{T_1 \cdot P_V}{2 \cdot U} \cdot \sqrt[4]{\frac{U}{4 \cdot E \cdot I}} = 0.08\ in$$ Track Deflection Ref #3, Fig. O-V

$$L_R := \frac{T_1 \cdot P_V \cdot S}{2} \cdot \left(\frac{U}{4 \cdot E \cdot I}\right)^{\frac{1}{4}} = 6.429\ kip$$ Rail Seat Load Ref #3, Fig. O-V

$$A_{TP} := TP_W \cdot TP_L = 66\ in^2$$ Area of tie plate

$$R := \frac{T_1 \cdot P_V \cdot S}{2 \cdot A_{TP}} \cdot \left(\frac{U}{4 \cdot E \cdot I} \right)^{\frac{1}{4}} = 97.406 \ \frac{lbf}{in^2}$$ Plate Pressure on tie

$$M := \frac{B_1 \cdot P_V}{4} \cdot \left(\frac{4 \cdot E \cdot I}{U} \right)^{\frac{1}{4}} = 234.704 \ in \cdot kip$$ Rail Bending Moment

$$F := \frac{B_1 \cdot P_V \cdot C}{4 \cdot I} \cdot \left(\frac{4 \cdot E \cdot I}{U} \right)^{\frac{1}{4}} = 8.347 \ ksi$$ Rail Bending Stress

$$P_a := \frac{T_1 \cdot P_V \cdot S}{L \cdot B} \cdot \left(\frac{U}{4 \cdot E \cdot I} \right)^{\frac{1}{4}} = 11.46 \ psi$$

$P_a = 79.011 \ kPa$ Static Pressure between crosstie and ballast.

Calculation steps have been provided at 144.6 kN (32.5 kips) of wheel load.

INPUT VARIABLES:

$V := 0\ mph$	Velocity (static conditions)
$D_w := 40\ in$	Wheel Diameter
$S := 20\ in$	Center to center tie spacing
$E := 30000000\ \frac{lbf}{in^2}$	Modulus of Rail
$I := 94.2\ in^4$	Moment of Inertia of Rail
$C := 3.35\ in$	Distance between rail neutral axis and location at which F is to be computed, usually at the rail base to maximize C.
$S_h := (23.7)\ in^3$	Section modulus of head (AREMA Figure 4-1-5).
$S_b := (28.2)\ in^3$	Section modulus of base (AREMA Figure 4-1-5).
$B := 11\ in$	Width of Tie
$L := 102\ in$	Length of Tie
$TP_W := 6\ in$	Width of Tie Plate
$TP_L := 11\ in$	Length of Tie Plate
$U := 4000\ \frac{lbf}{in^2}$	Track Modulus
$P_c := 2000\ psf$	Allowable Bearing Pressure of the Subgrade

CALCULATION:

$P_S := 32.5\ kip$ — Single (Static) Wheel Load of Car

$\theta := \frac{0.0052 \cdot V}{D_w}$ $\quad \theta := 0$ — Theta will be zero since we are looking at static conditions.

$P_V := P_S + \theta \cdot P_S = 32.5\ kip$ — Single (Dynamic) Wheel Load of Design Locomotive, which is equal to static wheel load since we are looking at static conditions.

$\alpha := 1$ — Since the velocity is less 40 km/hr.

$P_{V1} := \frac{P_V}{1\ kip} \cdot 1000 = 3.25 \cdot 10^4$

$W_0 := \left(315 - \frac{21200}{\left(\frac{P_{V1}}{1120}\right) \cdot \alpha + 67}\right) \cdot 1\ \frac{lb}{yd} = 94.208\ \frac{lb}{yd}$ — Minimum Rail Weight per EQ 6-5 (Ref. TI 850-02)

$X_1 := \frac{\pi}{4} \cdot \left(\frac{4 \cdot E \cdot I}{U}\right)^{\frac{1}{4}} = 32.202\ in$

$X_2 := X_1 \cdot 3 = 96.606\ in$

$D_{12} := 8\ ft + 6\ in = 102\ in$

$D_{23} := (59\ ft + 6\ in) - D_{12} = 612\ in$

$D_{34} := D_{12} = 102\ in$

To be persistent, inspection car's wheel dimensions are used for all calculations.

$$a := \frac{D_{12}}{X_2} = 1.056 \qquad d := \frac{D_{12}}{X_1} = 3.168$$

$$\frac{D_{23}}{X_2} = 6.335 \qquad \frac{D_{23}}{X_1} = 19.005$$

$$b := \frac{D_{12} + D_{23}}{X_2} = 7.391 \qquad e := \frac{D_{12} + D_{23}}{X_1} = 22.173$$

$$c := \frac{D_{12} + D_{23} + D_{34}}{X_2} = 8.447 \qquad f := \frac{D_{12} + D_{23} + D_{34}}{X_1} = 25.34$$

$$\begin{bmatrix} 0 \\ a \\ b \\ c \end{bmatrix} = \begin{bmatrix} 0 \\ 1.056 \\ 7.391 \\ 8.447 \end{bmatrix} \qquad \begin{bmatrix} 1 \\ -0.01 \\ 0 \\ 0 \end{bmatrix}$$ From Ahlf Graph

$$T_1 := 1 - 0.01 + 0 + 0 = 0.99$$

$$\begin{bmatrix} 0 \\ d \\ e \\ f \end{bmatrix} = \begin{bmatrix} 0 \\ 3.168 \\ 22.173 \\ 25.34 \end{bmatrix} \qquad \begin{bmatrix} 1 \\ -0.14 \\ 0 \\ 0 \end{bmatrix}$$ From Ahlf Graph

$$B_1 := 1 - 0.14 + 0 + 0 = 0.86$$

$$Y := \frac{T_1 \cdot P_V}{2 \cdot U} \cdot \sqrt[4]{\frac{U}{4 \cdot E \cdot I}} = 0.098\ in$$ Track Deflection Ref #3, Fig. O-V

$$L_R := \frac{T_1 \cdot P_V \cdot S}{2} \cdot \left(\frac{U}{4 \cdot E \cdot I}\right)^{\frac{1}{4}} = 7.847\ kip$$ Rail Seat Load Ref #3, Fig. O-V

$$A_{TP} := TP_W \cdot TP_L = 66\ in^2$$ Area of tie plate

$$R := \frac{T_1 \cdot P_V \cdot S}{2 \cdot A_{TP}} \cdot \left(\frac{U}{4 \cdot E \cdot I} \right)^{\frac{1}{4}} = 118.9 \ \frac{lbf}{in^2}$$ Plate Pressure on tie

$$M := \frac{B_1 \cdot P_V}{4} \cdot \left(\frac{4 \cdot E \cdot I}{U} \right)^{\frac{1}{4}} = 286.494 \ in \cdot kip$$ Rail Bending Moment

$$F := \frac{B_1 \cdot P_V \cdot C}{4 \cdot I} \cdot \left(\frac{4 \cdot E \cdot I}{U} \right)^{\frac{1}{4}} = 10.188 \ ksi$$ Rail Bending Stress

$$P_a := \frac{T_1 \cdot P_V \cdot S}{L \cdot B} \cdot \left(\frac{U}{4 \cdot E \cdot I} \right)^{\frac{1}{4}} = 13.988 \ psi$$

$P_a = 96.445 \ kPa$ Static Pressure between crosstie and ballast.

APPENDIX C – MATLAB BANDWIDTH FILTERING SCRIPT

The same script was used by Watts and Rose (2018) in their research. The script was written in MATLAB R2021b (The Math Works 2021).

```
%Welcome to Program Load in the pressure data. The filepath can be
%found by opening the properties of the specific file. Make sure
to use
%forward slashes instead of the standard backslash.
clc
clear all
close all
disp('Welcome')
prompt ='Please enter train name and date ';
x=input(prompt,'s');
trainname= (x);
prompt = 'Enter the path:';
x = input(prompt,'s');
addpath(x);
Train1=xlsread(x);
disp('Please wait...')
%Define your variables. In this case, we need to define the signal
of
%each pressure cell and the corresponding time domain.
c29 = Train1(:,1);  % Cell 29
c24 = Train1(:,2);  % Cell 24
c28 = Train1(:,3);  % Cell 28
c26 = Train1(:,4);  % Cell 26
c87 = Train1(:,5);  % Cell 87
c89 = Train1(:,6);  % Cell 89

% Cell 91 and Cell 25 are the 7th and 8th columns, but do not
provide
% significant results to look at.
% Sample Rate is 2000/sec. Each table entry is a sample.
time = [0:length(Train1)-1]/2000;

run=1; %will run the first test
while run==1
    prompt ='Please enter Cell(c29,c24,c28,c26,c87,c89) ';
    x=input(prompt);
    cell=(x);

    % Then, if you want to plot the raw signal output, one must
define a
    % new figure and call out the variables needed to be
displayed.
```

```
    f1=figure;                                  % Creates a new
figure

    plot(time,cell);                           % Creates the plot.
Can be found in
    % a new window.
    title(trainname);                           % Add title to the
figure
    xlabel('Time (s)');                        % Add x-axis label
    ylabel('Pressure (psi)');                  % Add y-axis label
    % Next, a spectrogram needs to be developed to determine the
    % appropriate filter to model the signal. The [s,f,t] function
returns
    % a spectrogram at the cyclical frequencies specified in f
    % (x,window,noverlap,f,fs). In other words, a fourier
trasnform is
    % performed and a heatmap is created to see the most dominant
    % frequencies.
    f2=figure
    [S,F,T] = spectrogram(cell,hamming(1024),1024-128,2048,2000);
    title(trainname);                           % Add title to the
figure
    imagesc(T,F,10*log10(abs(S)));axis('xy');colorbar

    % Based on the spectrogram, the most dominant energy/frequency
is seen
    % at 80 Hz. This will be the frequency used to filter the
signal. Most
    % trains are between 60 and 80 Hz.
    % Develop a bandwidth filter at 80 Hz
    prompt ='Enter bandwidth(typ. between 60 Hz and 80Hz)';
    x=input(prompt);
    bandwidth=(x);
    b = fir1(512,[bandwidth/4000]);
    %Hz has to be divided by twice
    % the sample rate
    nflow = filtfilt(b,1,cell);
    % The filtfilt function passes through
    % the signal twice
    specs=0;
```

```
    size1=0;
    while specs<1
        while size1<1
            %Get Min Peak Distance
            prompt ='MinPeakDistance(Typ .1)?';
            x=input(prompt);
            MinPeakDistance= (x);

            %Get Min Peak Height
            prompt ='MinPeakHeight(Typ 1)?';
            x=input(prompt);
            MinPeakHeight= (x);

            %Get Min Peak Prominence
            prompt ='MinPeakProminence(Typ .4)?';
            x=input(prompt);
            MinPeakProminencet= (x);


            f3=figure
            plot(time,cell);

            hold on;                                    % Need to
define this to superimpose the
            % filtered signal
            csvwrite('time.txt', time)
            csvwrite('nflow.txt', nflow)
            plot(time,nflow,'r','Linewidth',1.5);   % Plot the
filtered signal

            % Now, we need to mark the axle pressures

            [pv,pl] =
findpeaks(nflow,2000,'MinPeakDistance',MinPeakDistance,'MinPeakHei
ght',MinPeakHeight,'MinPeakProminence',MinPeakProminencet);

            % The function above will need to be played with for
each train as
            % speed varies. Don't spend too much time on this.
Typically 95% of the
            % heavy vehicles will be loacted. Only about 50-60% of
the empty cars
```

```
            % do.

            plot(pl,pv,'xk','MarkerSize',10);         % Plot to
see where these peaks are located.

            size (pv)                                 % Check to
see how many peaks/axles. In this case
            % these are 134 reported. Most likely more need to be
added afterwards.

            prompt ='Does number of peaks look right?(1=yes 0
=no)';
            x=input(prompt);
            size1= (x);
        end
        % Define the csv to export

        % Time column for each peak
        prompt ='Please enter value(2=c29,3=c24,4=c28,5=c26,6
=c87,7=c89) ';
        x=input(prompt);
        u=(x);
        [p(:,u), p(:,1)] =
findpeaks(nflow,2000,'MinPeakDistance',MinPeakDistance,'MinPeakHei
ght',MinPeakHeight,'MinPeakProminence',MinPeakProminencet);

        % Pressure Value for each peak

        [v(:,u), v(:,1)] =
findpeaks(nflow,2000,'MinPeakDistance',MinPeakDistance,'MinPeakHei
ght',MinPeakHeight,'MinPeakProminence',MinPeakProminencet);

        % Check to see you have the correct matrix dimensions
        size (v)

        prompt ='Are matrix dimension correct? Save csv file?(1
=yes 0=no)';
        x=input(prompt);
        specs= (x);
    end
```

```
    % Create CSV
    prompt ='Please Name excel sheet(end with .csv or will fail)
';
    x=input(prompt,'s');
    cellname=(x);
    csvwrite(cellname,v)

    % CSV file is written in the folder you are currently working
in.
    % Retrive and adjust as needed.

    prompt ='Would you like to run a different cell (1=yes 0=no)';
    x=input(prompt);
    run=(x);
end
```

APPENDIX D – MATHCAD AFFACTED DISTANCE CALCULATIONS EXAMPLE SHEET

Calculations steps of affected distance have been provided in the following figures. Mathcad 7.0 Prime (PTC 2021) has been used for the calculations.

30 mph at 80 Hz

Times for peak pressures determined by using MATLAB bandwidth filtering tools:

$t_1 := 0.2135\ s$

$t_2 := 0.356\ s$

$t_3 := 0.512\ s$ LOCOMOTIVE

$t_4 := 1.2435\ s$

$t_5 := 1.399\ s$

$t_6 := 1.5435\ s$

$t_7 := 1.849\ s$

$t_8 := 2.028\ s$

$t_{10} := 2.8875\ s$ DOTX 218

$t_{11} := 3.0655\ s$

$t_9 := 2.66\ s$ DEPLOYABLE

$t_{12} := 3.427\ s$

$t_{13} := 3.616\ s$ DOTX 220

$t_{14} := 4.792\ s$

$t_{15} := 4.983\ s$

The time bogies start and end feeling the pressures determined by using exported Excel file.
The pressures over 0.1 kPa as used as reference to decide to feeling pressure times:

$t_{start\_bogie\_1} := 0.116\ s$

$t_{end\_bogie\_1} := 0.62\ s$

LOCOMOTIVE

$t_{start\_bogie\_2} := 1.152\ s$

$t_{end\_bogie\_2} := 1.6475\ s$

$t_{start\_bogie\_3} := 1.765\ s$

$t_{end\_bogie\_3} := 2.1225\ s$

DOTX 218

$t_{start\_bogie\_5} := 2.79\ s$

$t_{end\_bogie\_5} := 3.1445\ s$

$t_{start\_bogie\_4} := 2.585\ s$

DEPLOYABLE

$t_{end\_bogie\_4} := 2.79\ s$

$t_{start\_bogie\_6} := 3.3365\ s$

$t_{end\_bogie\_6} := 3.723\ s$

$t_{start\_bogie\_7} := 4.6995\ s$

DOTX 220

$t_{end\_bogie\_7} := 5.081\ s$

$c_L := 74.875\ in$

$c_{218} := 64\ in$

$c_{220} := 102\ in$

Distances between wheels:

$L_{between\_1and2} := 79.6250\ in$ $L_{between\_1and2} = (2.022 \cdot 10^3)\ mm$

$L_{between\_2and3} := 83.75\ in$ $L_{between\_2and3} = (2.127 \cdot 10^3)\ mm$

$L_{between\_3and4} := 382.5\ in$ $L_{between\_3and4} = (9.716 \cdot 10^3)\ mm$

$L_{between\_4and5} := 83.75\ in$ $L_{between\_4and5} = (2.127 \cdot 10^3)\ mm$

$L_{between\_5and6} := 79.6250\ in$ $L_{between\_5and6} = (2.022 \cdot 10^3)\ mm$

$L_{between\_6and7} := c_L + c_{218} = 138.875\ in$ $L_{between\_6and7} = (3.527 \cdot 10^3)\ mm$

$L_{between\_7and8} := 98\ in$ $L_{between\_7and8} = (2.489 \cdot 10^3)\ mm$

$L_{between\_8and9} := 328.5\ in$ $L_{between\_8and9} = (8.344 \cdot 10^3)\ mm$

$L_{between\_9and10} := 120.5\ in$ $L_{between\_9and10} = (3.061 \cdot 10^3)\ mm$

$L_{between\_10and11} := 98\ in$ $L_{between\_10and11} = (2.489 \cdot 10^3)\ mm$

$L_{between\_11and12} := c_{218} + c_{220} = 166\ in$ $L_{between\_11and12} = (4.216 \cdot 10^3)\ mm$

$L_{between\_12and13} := 102\ in$ $L_{between\_12and13} = (2.591 \cdot 10^3)\ mm$

$L_{between\_13and14} := 612\ in$ $L_{between\_13and14} = (1.554 \cdot 10^4)\ mm$

$L_{between\_14and15} := 102\ in$ $L_{between\_14and15} = (2.591 \cdot 10^3)\ mm$

$$V_{1\_2} := \frac{L_{between\_1and2}}{t_2 - t_1} = 31.748\ mph$$

$$V_{2\_3} := \frac{L_{between\_2and3}}{t_3 - t_2} = 30.503\ mph$$

$$V_{3\_4} := \frac{L_{between\_3and4}}{t_4 - t_3} = 29.71\ mph$$

$$V_{4\_5} := \frac{L_{between\_4and5}}{t_5 - t_4} = 30.601\ mph$$

$$V_{5\_6} := \frac{L_{between\_5and6}}{t_6 - t_5} = 31.309\ mph$$

$$V_{6\_7} := \frac{L_{between\_6and7}}{t_7 - t_6} = 25.829\ mph$$

$$V_{7\_8} := \frac{L_{between\_7and8}}{t_8 - t_7} = 31.107\ mph$$

$$V_{8\_9} := \frac{L_{between\_8and9}}{t_9 - t_8} = 29.533\ mph$$

$$V_{9\_10} := \frac{L_{between\_9and10}}{t_{10} - t_9} = 30.095\ mph$$

$$V_{10\_11} := \frac{L_{between\_10and11}}{t_{11} - t_{10}} = 31.282\ mph$$

$$V_{11\_12} := \frac{L_{between\_11and12}}{t_{12} - t_{11}} = 26.091\ mph$$

$$V_{12\_13} := \frac{L_{between\_12and13}}{t_{13} - t_{12}} = 30.664\ mph$$

$$V_{13\_14} := \frac{L_{between\_13and14}}{t_{14} - t_{13}} = 29.569\ mph$$

$$V_{14\_15} := \frac{L_{between\_14and15}}{t_{15} - t_{14}} = 30.343\ mph$$

Estimated actual speed:

$$V := 29.88457\ mph \qquad V = 48.095\ \frac{km}{hr}$$

Affected distances due to wheel loadings and speed. These values are converted to SI units and used to develop functions.

Locomotive:

$$a1 := V \cdot \left(t_1 - t_{start\_bogie\_1}\right) = 51.282\ in$$

$$b1 := V \cdot \left(t_{end\_bogie\_1} - t_3\right) = 56.805\ in$$

$$c1 := V \cdot \left(t_4 - t_{start\_bogie\_2}\right) = 48.126\ in$$

$$d1 := V \cdot \left(t_{end\_bogie\_2} - t_6\right) = 54.701\ in$$

DOTX 218:

$$a := V \cdot \left(t_7 - t_{start\_bogie\_3}\right) = 44.181\ in$$

$$b := V \cdot \left(t_{end\_bogie\_3} - t_8\right) = 49.704\ in$$

$$c := V \cdot \left(t_{10} - t_{start\_bogie\_5}\right) = 51.282\ in$$

$$d := V \cdot \left(t_{end\_bogie\_5} - t_{11}\right) = 41.552\ in$$

DOTX 220:

$$a := V \cdot \left(t_{12} - t_{start\_bogie\_6}\right) = 47.6\ in$$

$$b := V \cdot \left(t_{end\_bogie\_6} - t_{13}\right) = 56.279\ in$$

$$c := V \cdot \left(t_{14} - t_{start\_bogie\_7}\right) = 48.652\ in$$

$$d := V \cdot \left(t_{end\_bogie\_7} - t_{15}\right) = 51.545\ in$$

CALCULATIONS BY TAKING THE DATA AS A REFERENCE

$xx := \text{READEXCEL}(\text{".\analyzed - 30.xlsx"}, \text{"Sheet1!A2:A3500"})$

$yy := \text{READEXCEL}(\text{".\analyzed - 30.xlsx"}, \text{"Sheet1!D2:D3500"})$

$W_{vehicle} := 395\ kip \qquad W_{vehicle} = (1.757 \cdot 10^3)\ kN$

$P_s := \frac{W_{vehicle}}{12} = 146.421\ kN \qquad V = 48.095\ \frac{km}{hr}$

$a_s := \left(-9.9922 \cdot \left(\frac{P_s}{1\ kN} \cdot 0.2193\right) + 1486.5\right) \cdot 1\ mm = 1165.65\ mm$

$b_s := \left(3.9915 \cdot \left(\frac{P_s}{1\ kN} \cdot 0.2193\right) + 1284.9\right) \cdot 1\ mm = 1413.067\ mm$

$c_s := \left(-18.104 \cdot \left(\frac{P_s}{1\ kN} \cdot 0.2193\right) + 1751.2\right) \cdot 1\ mm = 1169.88\ mm$

$d_s := \left(31.06 \cdot \left(\frac{P_s}{1\ kN} \cdot 0.2193\right) + 481.99\right) \cdot 1\ mm = 1479.328\ mm$

$a_r := -0.0004 \cdot \frac{V}{\frac{km}{hr}} + 1 = 0.981 \qquad b_r := 0.0005 \cdot \frac{V}{\frac{km}{hr}} + 1 = 1.024$

$c_r := -0.0002 \cdot \frac{V}{\frac{km}{hr}} + 1 = 0.99 \qquad d_r := 0.0002 \cdot \frac{V}{\frac{km}{hr}} + 1 = 1.01$

$a_d := a_r \cdot a_s = 1143.225\ mm$

$b_d := b_r \cdot b_s = 1447.048\ mm$

$c_d := c_r \cdot c_s = 1158.627\ mm$

$d_d := d_r \cdot d_s = 1493.557\ mm$

$L_{bogie\_1} := L_{between\_1and2} + L_{between\_2and3} + (a_d + b_d) = 265.354\ in$ $L_{bogie\_1} = (6.74 \cdot 10^3)\ mm$

$L_{bogie\_2} := L_{between\_4and5} + L_{between\_5and6} + (c_d + d_d) = 267.792\ in$ $L_{bogie\_2} = (6.802 \cdot 10^3)\ mm$

$$t_{bogie\_1} := \frac{L_{bogie\_1}}{V} = 0.505\ s$$

$$t_{bogie\_2} := \frac{L_{bogie\_2}}{V} = 0.509\ s$$

Calculating AMPLITUDE:

$$P_{static} := \frac{W_{vehicle}}{12} = 32.917\ kip$$

<= Static wheel load

$P_{static} = 146.421\ kN$

$$\sigma_{static} := \left(6.1137 \cdot \frac{P_{static} \cdot 0.2193}{1\ kip} - 17.407\right) psi = 26.726\ psi$$

$\sigma_{static} = 184.266\ kPa$

$$\sigma_s := \left(9.5073 \cdot \left(\frac{P_s \cdot 0.2193}{1\ kN}\right) - 120.02\right) \cdot 1\ kPa = 185.26\ kPa$$

$m_{USA} := -0.0035$

$m_{SI} := -0.0022$

$$\sigma_d := \sigma_s \cdot \left(m_{SI} \cdot \frac{V}{\frac{km}{hr}} + 1\right) = 165.658\ kPa$$

Calculating the time between bogies:

$$L_{between\_bogies} := L_{between\_3and4} - b_d - c_d = (7.11 \cdot 10^3)\ mm$$

$$t_{between\_bogies} := \frac{L_{between\_bogies}}{V} = 0.532\ s$$

$$t_0 := 0.116\ s \qquad t := \frac{t_0}{s} = 0.116$$

$$t_1 := \frac{t_{bogie\_1}}{s} + t = 0.621$$

$$t_2 := \frac{t_{bogie\_1} + t_{between\_bogies}}{s} + t = 1.153$$

$$t_3 := \frac{t_{bogie\_1} + t_{between\_bogies} + t_{bogie\_2}}{s} + t = 1.662$$

$$t_4 := \frac{t_{bogie\_1} + t_{between\_bogies} + t_{bogie\_2}}{s} + t + t = 1.778$$

PROGRAM:

$$f(x) := \begin{cases} \text{if } (t \le x) \wedge (x \le t_1) \\ \quad A_1 \\ \text{else if } (-0.05 \le x) \wedge (x \le t) \\ \quad 0 \\ \text{else if } (x > t_1) \wedge (x \le t_2) \\ \quad 0 \\ \text{else if } (t_2 \le x) \wedge (x \le t_3) \\ \quad A_1 \\ \text{else if } (t_3 \le x) \wedge (x \le t_4) \\ \quad 0 \end{cases}$$

APPENDIX E – PYHTON 3.0 THE SQUARE WAVE THEORY ALGORITHM SCRIPT

The program algorithm has been provided in the following figures. The script has been written in Python 3.0 (Python Software Foundation 2022).

```
import numpy as np
import pandas as pd
import matplotlib.pyplot as plt

start_offset_x = 0.1
start_offset_y = 0

#Distribution load factor at the crosstie-ballast interface:
global_distributionFactor = 0.2193

#Reading Input Excel File:
def ReadExcelandCalculate(x, y,f):

   x.append(0)
   y.append(0)
   x.append(0+start_offset_x)
   y.append(0+start_offset_y)

   inputs = pd.read_excel("input.xlsx")
   df = pd.DataFrame(inputs)

   for index, row in df.iterrows():
      f.write("--------------------------------"+'\n')
      print("--------------------------------"+'\n')
      val = "Excel Row: " +str(index+2)+'\n'
      print(val)
      f.write(val)
      f.write(row["CAR_TYPE"]+'\n')
      print(row["CAR_TYPE"])
      if row["CAR_TYPE"] == "Locomotive" :

         RBWHEL =[]
         RBWHEL.append(row["DB12"])
         RBWHEL.append(row["DB23"])
         RBWHEL.append(row["DB34"])
         RBWHEL.append(row["DB45"])
         RBWHEL.append(row["DB56"])

         LOCDISTANCES =  row["LOFC"] + row["LOBC"]+ row["DBHFW"] +
row["DBELW"]

         x,y=CalculateForLocomotive( x,
                                     y,
                                     row["SPEED"],
                                     row["VEHICLE_WEIGHT"],
                                     row["NAX"],
                                     RBWHEL,
                                     LOCDISTANCES,
                                     f)
      if row["CAR_TYPE"] == "Car" :

         RBWHEL =[]
         RBWHEL.append(row["DB12"])
         RBWHEL.append(row["DB23"])
         RBWHEL.append(row["DB34"])
         RBWHEL.append(row["DB45"])
         RBWHEL.append(row["DB56"])
```

```
        LOCDISTANCES =  row["LOFC"] + row["LOBC"]+ row["DBHFW"] +
row["DBELW"]

        x,y=CalculateForCar(      x,
                                  y,
                                  row["SPEED"],
                                  row["VEHICLE_WEIGHT"],
                                  row["NAX"],
                                  RBWHEL,
                                  LOCDISTANCES,
                                  f
                                  )
      f.write("--------------------------------\n")
      print("--------------------------------\n")

   return x,y


#Steps for locomative:
def CalculateForLocomotive(x, y, SPEED, VEHICLE_WEIGHT, NAX , RBWHEL,
LOCDISTANCES,f):# ,WHEEL_DIAMETER ,ALPHA
   P_static = calculate_Pstatic(VEHICLE_WEIGHT, NAX,f)
   #Calculating static pressures:
   PRstatic = 9.5073*(P_static*global_distributionFactor)-120.02
   #Slope
   ml= -0.0022
   Vspeed = calculate_Vspeed(SPEED,f)
   #Calculating dynamic pressures:
   PRdynamic = PRstatic * (ml * Vspeed +1)

   #Calculating affacted static distances:
   a_staticDistance = (-9.9922 * (P_static * global_distributionFactor)) +
1486.5
   b_staticDistance = (3.9915 * (P_static * global_distributionFactor)) +
1284.9
   c_staticDistance = (-18.104 * (P_static * global_distributionFactor)) +
1751.2
   d_staticDistance = (31.06 * (P_static * global_distributionFactor)) +
481.99

   #Calculating ratios:
   a_ratio = (-0.0004 * Vspeed) + 1.0
   b_ratio = (0.0005 * Vspeed) + 1.0
   c_ratio = (-0.0002 * Vspeed) + 1.0
   d_ratio = (0.0002 * Vspeed) + 1.0

   #Calculating affacted dynamic distances:
   a_dynamicDistance = a_ratio * a_staticDistance
   b_dynamicDistance = b_ratio * b_staticDistance
   c_dynamicDistance = c_ratio * c_staticDistance
   d_dynamicDistance = d_ratio * d_staticDistance

   def calculate_bogieLengthandTime(ranges_between_wheels, input_speed,f):
      if ranges_between_wheels[3] == 0 or ranges_between_wheels[4] == 0:  #4
axles
         bogie_length_1 = (ranges_between_wheels[0] + (a_dynamicDistance +
```

```
b_dynamicDistance)) * 0.000001
         bogie_length_2 = (ranges_between_wheels[2] + (c_dynamicDistance +
d_dynamicDistance)) * 0.000001
      else:  #6 axles
         bogie_length_1 = (ranges_between_wheels[0] +
ranges_between_wheels[1] + (
                  a_dynamicDistance + b_dynamicDistance)) * 0.000001
         bogie_length_2 = (ranges_between_wheels[3] +
ranges_between_wheels[4] + (
                  c_dynamicDistance + d_dynamicDistance)) * 0.000001
      #Calculating bogie times:
      bogie_1_time = (bogie_length_1 / input_speed) * 3600
      bogie_2_time = (bogie_length_2 / input_speed) * 3600

      print(
         "bogie_length_1 : {} | bogie_length_2 : {} \nbogie_1_time : {} |
bogie_2_time : {} ".format(bogie_length_1,

bogie_length_2,

bogie_1_time,

bogie_2_time))


      f.write(
         "bogie_length_1 : {} | bogie_length_2 : {} \nbogie_1_time : {} |
bogie_2_time : {} ".format(bogie_length_1,

bogie_length_2,

bogie_1_time,

bogie_2_time)+'\n')
      return bogie_length_1, bogie_length_2, bogie_1_time, bogie_2_time

   #Calculating times between bogies:
   def calculate_BetweenBogiesTime(ranges_between_wheels, input_speed,f):
      if ranges_between_wheels[3] == 0 or ranges_between_wheels[4] == 0:  # 4
axles
         bogie_btween = (ranges_between_wheels[1] - (c_dynamicDistance +
b_dynamicDistance)) * 0.000001
         between_bogie_length = ranges_between_wheels[1]
      else:  # 6 axles
         bogie_btween = (ranges_between_wheels[2] - (c_dynamicDistance +
b_dynamicDistance)) * 0.000001
         between_bogie_length = ranges_between_wheels[2]

      between_time = (bogie_btween / input_speed) * 3600

      f.write("between_bogie_length : {} \nBetweenTime : {}
".format(bogie_btween, between_time)+'\n')
      print("between_bogie_length : {} \nBetweenTime : {}
".format(bogie_btween, between_time))
      return between_bogie_length, between_time

   #Calculating times between locomotives/cars:
```

```
   def calculate_BetweenLocosTime(loc_distances, input_speed,f):
      BetweenLocosTime = ((loc_distances - (
               d_dynamicDistance + a_dynamicDistance)) * 0.000001) /
input_speed * 3600
      print(" loc_distances: {} \n input_speed: {} \n BetweenLocosTime:
{}".format(loc_distances, input_speed,

BetweenLocosTime))

      f.write(" loc_distances: {} \n input_speed: {} \n BetweenLocosTime:
{}".format(loc_distances, input_speed,

BetweenLocosTime)+'\n')
      return loc_distances, BetweenLocosTime

   bogietime = calculate_bogieLengthandTime(RBWHEL,SPEED,f)
   betweenbogiestime = calculate_BetweenBogiesTime(RBWHEL,SPEED,f)
   between_locos_time = calculate_BetweenLocosTime(LOCDISTANCES,SPEED,f)

   #Calculating amplitude (dynamic pressures):
   AMPLITUDE=PRdynamic

   final_index= len(x)-1

   x.append(x[final_index]+bogietime[2])
   y.append(AMPLITUDE)
   final_index+=1
   x.append(x[final_index]+betweenbogiestime[1])
   y.append(0)
   final_index+=1
   x.append(x[final_index]+bogietime[3])
   y.append(AMPLITUDE)
   final_index+=1
   x.append(x[final_index]+between_locos_time[1])
   y.append(0)
   final_index+=1

   return x,y

#Steps for car:
def CalculateForCar(x, y, SPEED, VEHICLE_WEIGHT, NAX, RBWHEL,
LOCDISTANCES,f): #, WHEEL_DIAMETER, ALPHA
   P_static = calculate_Pstatic(VEHICLE_WEIGHT, NAX,f)
   #Calculating static pressures:
   PRstatic = 9.5073*(P_static*global_distributionFactor)-120.02
   #Slope
   ml= -0.0022
   Vspeed = calculate_Vspeed(SPEED,f)
   #Calculating dynamic pressures:
   PRdynamic = PRstatic * (ml * Vspeed +1)

   a_staticDistance = (-9.9922 * (P_static * global_distributionFactor)) +
1486.5
   b_staticDistance = (3.9915 * (P_static * global_distributionFactor)) +
1284.9
   c_staticDistance = (-18.104 * (P_static * global_distributionFactor)) +
1751.2
```

```
   d_staticDistance = (31.06 * (P_static * global_distributionFactor)) +
481.99

   #Calculating ratios:
   a_ratio = (-0.0004 * Vspeed) + 1.0
   b_ratio = (0.0005 * Vspeed) + 1.0
   c_ratio = (-0.0002 * Vspeed) + 1.0
   d_ratio = (0.0002 * Vspeed) + 1.0

   #Calculating affacted dynamic distances:
   a_dynamicDistance = a_ratio * a_staticDistance
   b_dynamicDistance = b_ratio * b_staticDistance
   c_dynamicDistance = c_ratio * c_staticDistance
   d_dynamicDistance = d_ratio * d_staticDistance

   def calculate_bogieLengthandTime(ranges_between_wheels, input_speed,f):
      if ranges_between_wheels[3] == 0 or ranges_between_wheels[4] == 0:  # 4
axels
         bogie_length_1 = (ranges_between_wheels[0] + (a_dynamicDistance +
b_dynamicDistance)) * 0.000001
         bogie_length_2 = (ranges_between_wheels[2] + (c_dynamicDistance +
d_dynamicDistance)) * 0.000001
      else:  # 6axels
         bogie_length_1 = (ranges_between_wheels[0] +
ranges_between_wheels[1] + (
                  a_dynamicDistance + b_dynamicDistance)) * 0.000001
         bogie_length_2 = (ranges_between_wheels[3] +
ranges_between_wheels[4] + (
                  c_dynamicDistance + d_dynamicDistance)) * 0.000001

      bogie_1_time = (bogie_length_1 / input_speed) * 3600
      bogie_2_time = (bogie_length_2 / input_speed) * 3600

      f.write(
         "bogie_length_1 : {} | bogie_length_2 : {} \nbogie_1_time : {} |
bogie_2_time : {} ".format(bogie_length_1,

bogie_length_2,

bogie_1_time,

bogie_2_time)+'\n')
      print(
         "bogie_length_1 : {} | bogie_length_2 : {} \nbogie_1_time : {} |
bogie_2_time : {} ".format(bogie_length_1,

bogie_length_2,

bogie_1_time,

bogie_2_time))
      return bogie_length_1, bogie_length_2, bogie_1_time, bogie_2_time

   def calculate_BetweenBogiesTime(ranges_between_wheels, input_speed,f):
      if ranges_between_wheels[3] == 0 or ranges_between_wheels[4] == 0:  # 4
axels
         bogie_btween = (ranges_between_wheels[1] - (c_dynamicDistance +
```

```
b_dynamicDistance)) * 0.000001
            between_bogie_length = ranges_between_wheels[1]
         else:  # 6axels
            bogie_btween = (ranges_between_wheels[2] - (c_dynamicDistance +
b_dynamicDistance)) * 0.000001
            between_bogie_length = ranges_between_wheels[2]

         between_time = (bogie_btween / input_speed) * 3600

         f.write("between_bogie_length : {} \nBetweenTime : {}
".format(bogie_btween, between_time)+'\n')
         print("between_bogie_length : {} \nBetweenTime : {}
".format(bogie_btween, between_time))
         return between_bogie_length, between_time

      def calculate_BetweenLocosTime(loc_distances, input_speed,f):
         BetweenLocosTime = ((loc_distances - (
                  d_dynamicDistance + a_dynamicDistance)) * 0.000001) /
input_speed * 3600
         print(" loc_distances: {} \n input_speed: {} \n BetweenLocosTime:
{}".format(loc_distances, input_speed,

BetweenLocosTime))

         f.write(" loc_distances: {} \n input_speed: {} \n BetweenLocosTime:
{}".format(loc_distances, input_speed,

BetweenLocosTime)+'\n')
         return loc_distances, BetweenLocosTime

      bogietime = calculate_bogieLengthandTime(RBWHEL,SPEED,f)
      betweenbogiestime = calculate_BetweenBogiesTime(RBWHEL,SPEED,f)
      between_locos_time = calculate_BetweenLocosTime(LOCDISTANCES,SPEED,f)

      AMPLITUDE=PRdynamic


      final_index= len(x)-1

      x.append(x[final_index]+bogietime[2])
      y.append(AMPLITUDE)
      final_index+=1
      x.append(x[final_index]+betweenbogiestime[1])
      y.append(0)
      final_index+=1
      x.append(x[final_index]+bogietime[3])
      y.append(AMPLITUDE)
      final_index+=1
      x.append(x[final_index]+between_locos_time[1])
      y.append(0)
      final_index+=1

      return x,y


#Converting the speed from the input Excel file to the integer
def calculate_Vspeed(input_speed,f):
```

```
    V_speed = input_speed
    print("Vspeed: {}".format(V_speed))
    f.write("Vspeed: {}".format(V_speed)+'\n')
    return V_speed

#Calculating static load:
def calculate_Pstatic(input_weight, input_axles_numbers,f):
    P_static = input_weight / (2 * input_axles_numbers)
    f.write("Pstatic: {}".format(P_static)+'\n')
    print("Pstatic: {}".format(P_static))
    return P_static


#Plotting the results:
def makeChart(x, y):
    plt.style.use('_mpl-gallery')
    # plot
    fig, ax = plt.subplots()

    ax.step(x, y, linewidth=4)

    ax.set(xlim=(0, 20), xticks=np.arange(0, 15, 1),
           ylim=(0, 300), yticks=np.arange(0, 250, 20))

    plt.xlabel('Time (s)')
    plt.ylabel('Pressure (kPa)')

    plt.show()

#The step for the output file:
def main():
    x = []
    y = []
    reportFile='report.txt'
    f= open(reportFile,'w+')

    x, y = ReadExcelandCalculate(x, y, f)

    col1 = 'Time (s)'
    col2 = 'Pressure (psi)'
    col3 = 'Time (s)'
    col4 = 'Pressure (psi)'
    tempData=np.zeros((2*len(x)-2,2))
    tempData[0,0]=x[0]
    tempData[-1,0]= x[-1]
    for i in range(1,len(x)-1):

        tempData[(2*i)-1,0]=x[i]
        tempData[2*i,0]=x[i]


        tempData[(2*i)-1,1]=y[i]
        tempData[2*i,1]=y[i+1]

    x_df = pd.DataFrame({col3:tempData[:,0],col4:tempData[:,1]})
    x_df.to_excel("output.xlsx", sheet_name= 'Data', index= False)
    f.close()
```

```
    makeChart(x, y)

if __name__ == "__main__":
    main()
```

APPENDIX F – EXCEL INPUT DESCRIPTIONS

The table presents the symbols and description of the Excel Input Worksheet of the Square Wave Algorithm.

DESCRIBTION	SYMBOL
DISTANCE FROM THE END TO FIRST WHEEL	DBEFW
DISTANCE FROM THE HEAD TO LAST WHEEL	DBHLW
BACK COUPLER LENGTH	LOBC
FRONT COUPLER LENGTH	LOFC
DISTANCE BETWEEN WHEEL #5 AND #6	DB56
DISTANCE BETWEEN WHEEL #4 AND #5	DB45
DISTANCE BETWEEN WHEEL #3 AND #4	DB34
DISTANCE BETWEEN WHEEL #2 AND #3	DB23
DISTANCE BETWEEN WHEEL #1 AND #2	DB12
NUMBER OF AXLES	NAX
VEHICLE SPEED	SPEED
VEHICLE WEIGHT	VEHICLE_WEIGHT
CAR ORDER	CAR_ORDER
CAR TYPE	CAR_TYPE

REFERENCES

Abbey, W. W. (1985). The Track Cyclopedia, p. 170. Omaha, NE: Simmons-Boardman Books, Inc. 1985, Print.

Ahlf R. E. (2003). Soil, Structure and Drainage Engineering for Railroads. February 10, 2003, University of Wisconsin, Madison, WI.

Al-Qadi, Xie, W., Jones, D. L., & Roberts, R. (2010). Development of a Time-frequency Approach to Quantify Railroad Ballast Fouling Condition using Ultra-wide Band Ground-penetrating Radar Data. The International Journal of Pavement Engineering, 11(4), 269–279. https://doi.org/10.1080/10298431003749766

American Railway Engineering Association (1980). Stress in Railroad Track – the Talbot Reports. Washington, DC: American Railway Engineering Association.

AREMA. (2018). Manual for Railway Engineering. Lanham, MD: American Railway Engineering and Maintenance of Way Association.

Chrismer, S., and Davis, D. (2000). Cost Comparisons of Remedial Methods to Correct Track Substructure Instability. Transportation Research Record, National Research Council, Washington, D.C., 1713: 10–15. doi:10.3141/1713-02.

Das, B. M., and Sivakugan, N. (2019). In principles of Foundation Engineering. Boston, MA: Cengage Learning.

Doyle, N. F (1980). Railway Track Design: A Review of Current Practice. BHP Melbourne Research 300 Laboratories, Bureau of Transport Economics, 1980.

Geokon. (2017). Model 3500 Series Instruction Manual. Lebanon, NH.

Transportation Technology Center, Inc., GEOTRACK (2021). Association of American Railroads. Colorado, United States of America.

Hay, W. W. (1982). Railroad engineering (2nd ed.). New York, NY: Wiley.

Huang, Liu, S., and Qiu, T. (2018). Identification of Railroad Ballast Fouling through Particle Movements. Journal of Geotechnical and Geoenvironmental Engineering, 144(4), 2818001. https://doi.org/10.1061/(ASCE)GT.1943-5606.0001846

Indraratna, B., and Ngo, T. (2018). Ballast Railroad Design: SMART-UOW Approach.

London: CRC Press: Taylor & Francis Group.

Indraratna, Ngo, N. T., Rujikiatkamjorn, C., and Vinod, J. S. (2011). Behavior of Fresh and Fouled Railway Ballast Subjected to Direct Shear Testing: Discrete Element Simulation. International Journal of Geomechanics, 14(1), 34–44. https://doi.org/10.1061/(ASCE)GM.1943-5622.0000264

Li, Hyslip, J., Sussmann, T., and Chrismer, S. (2016). Railway Geotechnics. Boca Raton, FL: CRC Press. https://doi.org/10.1201/b18982

Liu, S., and Rose, J.G. (2013). KENTRACK 4.0: A Railway Trackbed Structural Design Program.

Lobo-Guerrero, and Vallejo, L. E. (2006). Discrete Element Method Analysis of Railtrack Ballast Degradation during Cyclic Loading. Granular Matter, 8(3), 195–204. https://doi.org/10.1007/s10035-006-0006-2

Powrie, W and Le Pen (2016). A Guide to Track Stiffness. University of Southampton Department of Civil and Enviromental Engineering.

PTC, Inc., Mathcad, version Prime 7 (Boston, MA: PTC, Inc., 2021), accessed March, 2021. https://www.mathcad.com/en

Python Software Foundation, Pyhton, version 3.0 (Delaware, DE: Python Software Foundation, 2022), accessed February, 2021. https://www.python.org/

Raymond, G. P. 1985. Analysis of Track Support and Determination of Track Modulus. Transportation Research Record, 1022, 80-90.

Rose, J.G. Clarke, D.B. Liu, L. and T.J. Watts (2018). Development of a Laboratory Test Method for Measuring Trackbed Pressure at the Tie/Ballast Interface. Paper 18-00592 TRB 97th Annual Meeting Online. Transportation Research Board, January, 2018, 12 pages.

Russell, E., Rose, J. G., Clarke D. B. (2020). In-Track Timber Crosstie-Ballast Interfacial Pressure Measurements for Revenue Freight Trains and DOTX 218/219 Test Train Operating Conditions. Proceeding paper AREMA RRB20 Symposium. American Railway Engineering and Maintenance of Way Association Railroad Road & Ballast, February, 2020, 21 pages.

Selig, E. T., and Waters, J. M. (1994). Track Geotechnology and Substructure Management. London: Thomas Telford Publications.

Smith, Steven (2013). Digital Signal Processing: A Practical Guide for Engineers and Scientists. Oxford: Elsevier Science and Technology, 2013. Print.

Stratman, Liu, Y., and Mahadevan, S. (2007). Structural Health Monitoring of Railroad Wheels Using Wheel Impact Load Detectors. Journal of Failure Analysis and Prevention, 7(3), 218–225. https://doi.org/10.1007/s11668-007-9043-3

Talbot, A. (1918). Stresses in Railroad Track (Progress Report No. 1). Washington, D.C.: American Railway Engineering Association.

Talbot, A. (1919). Stresses in Railroad Track (Progress Report No. 2). Washington, D.C.: American Railway Engineering Association.

Talbot, A. (1940). Stresses in Railroad Track - The Talbot Reports. Washington, D.C.: American Railway Engineering Association.

The Math Works, Inc., MATLAB, version 2021b (Natick, MA: The Math Works, Inc., 2021), accessed December, 2021. https://www.mathworks.com/

Thompson, Clarke, D. B., and Rose, J. G. (2020). Modeling Crosstie-Ballast Load Distribution in a Railroad Trackbed using a Linear-Elastic Analysis. Transportation Research Record, 2674(11), 76–86. https://doi.org/10.1177/0361198120937962

Timoshenko, S. 1927. Proceedings Second International Congress of Applied Mechanics: Methods of analysis of statical and dynamical stresses in rails. In Proc: Zurich. 407-418

Unluoglu H. A., Bryson L. S., and Rose J. G. (2022). Predicting Dynamic Contact Pressure at Crosstie-ballast Interface Based on Basic Information of Trains. Lexington, KY (In Progress).

Van Dyk, B. J., Edwards, J. R., Dersch, M. S., Ruppert, C. J., & Barkan, C. P. L. (2013). Evaluation of dynamic and impact wheel load factors and their application in design processes. Paper 14-4714 TRB 93rd Annual Meeting. Transportation Research Board, November, 2013, 19 pages. 2014_TRB_Van_Dyk_et_al_Dynamic_and_Impact_Factors.pdf (illinois.edu)

Wang, H., Zeng, L.-L., Bian, X., & Hong, Z.-S. (2020). Train Moving Load-Induced Vertical Superimposed Stress at Ballasted Railway Tracks. Advances in Civil Engineering, 2020, 1–11. https://doi.org/10.1155/2020/3428395

Watts T., and Rose, J. G. (2018). Direct Measurement of Crosstie-ballast Interface Pressures Using Granular Material Pressure Cells, Master's Thesis, University of Kentucky. https://doi.org/10.13023/etd.2018.440

VITA

Habib Abdil Unluoglu was born in Mugla, Turkey. His parents are Aydin and Sati Unluoglu. He completed his elementary and secondary education in his hometown. Upon graduating from high school in May 2013, he enrolled at the Karabuk University in Turkey. There he received a Bachelor of Science Degree in Mechanical Engineering, Railway Systems Engineering in June 2018. In 2020, he enrolled in the University of Kentucky, English as a Second Language program. He began work on his Master's Degree in Civil Engineering in the Fall of 2020, selecting the thesis MSCE program option. He was the Teaching Assistant of Prof. Jerry G. Rose for Railroad Facilities Design and Analysis, a testament to the work Habib has completed in his time as a Master's Student.